BIOMEDICAL PHOTONICS

BIOMEDICAL PHOTONICS –
research and practice, peer-reviewed, multidisciplinary journal.
The journal is issued 4 times per year.
The circulation – 1000 copies., on a quarterly basis.

The journal is included into the List of peer-reviewed science press of the State Commission for Academic Degrees and Titles of Russian Federation
The journal is indexed in the international abstract and citation database – Scopus.

The publisher «Agentstvo MORE».
Moscow, Khokhlovskiy lane, 9

Editorial staff:

Chief of the editorial staff	Ivanova-Radkevich V.I.
Science editor professor	Mamontov A.S.
Literary editor	Moiseeva R.N.
Translators	Kalyagina N.A.
Computer design	Kreneva E.I.
Desktop publishing	Shalimova N.M.

The Address of Editorial Office:
Russia, Moscow, 2nd Botkinskiy proezd, 3
Tel. 8 (495) 945–86–60
www: PDT-journal.com
E-mail: PDT-journal@mail.ru

Corresponding to:
125284, Moscow, p/o box 13

Registration certificate ПИ № ФС 77–51995, issued on 29.11.2012 by the Federal Service for Supervision of Communications, Information Technology, and Mass Media of Russia

The subscription index of «Rospechat» agency – 70249

BIOMEDICAL PHOTONICS

BIOMEDICAL PHOTONICS –
научно-практический, рецензируемый,
мультидисциплинарный журнал.
Выходит 4 раза в год.
Тираж – 1000 экз., ежеквартально.

Входит в Перечень ведущих рецензируемых научных журналов ВАК РФ.
Индексируется в международной реферативной базе данных Scopus.

Издательство «Агентство МОРЕ».
Москва, Хохловский пер., д. 9

Редакция:

Зав. редакцией	Иванова-Радкевич В.И.
Научный редактор	проф. Мамонтов А.С.
Литературный редактор	Моисеева Р.Н.
Переводчики	Калягина Н.А.
Компьютерный дизайн	Кренева Е.И.
Компьютерная верстка	Шалимова Н.М.

Адрес редакции:
Россия, Москва, 2-й Боткинский пр., д. 3
Тел. 8 (495) 945–86–60
www: PDT-journal.com
E-mail: PDT-journal@mail.ru

Адрес для корреспонденции:
125284, Москва, а/я 13

Свидетельство о регистрации ПИ
№ ФС 77–51995, выдано 29.11.2012 г.
Федеральной службой по надзору в сфере связи, информационных технологий и массовых коммуникаций (Роскомнадзор)

Индекс по каталогу агентства «Роспечать» – 70249

ORIGINAL ARTICLES

ОРИГИНАЛЬНЫЕ СТАТЬИ

USE OF ENDOGENOUS PIGMENT ANALYTES TO ASSESS THE INVASIVE POTENTIAL OF SUPERFICIAL SKIN MELANOMAS

Borisov A.V.[1], Chernov I.A.[1], Avdalyan A.M.[2], Timofeev S.E.[2], Ronzin A.V.[2], Nichiporov A.I.[2], Kukushkin V.I.[3], Kirillov Yu.A.[1,2,4]
[1]Tyumen State Medical University, Tyumen, Russia
[2]Moscow Multidisciplinary Clinical Center "Kommunarka", Moscow, Russia
[3]Institute of Solid State Physics of the Russian Academy of Sciences, Chernogolovka, Russia
[4]Petrovsky National Research Centre of Surgery, Moscow, Russia

Abstract

Cutaneous melanoma, which accounts for 72-80% of all diagnosed tumors developing from melanin-producing tissue, is an example of a malignancy whose initiation and development, with rare exceptions, are associated with the realization of endogenous pigmentations in the morphological substrate of the tumor. However, the existing diagnostic paradigm for superficial cutaneous melanomas does not take into account the significance of endogenous pigmentations in assessing the tumor's invasive capacity. This article examines the relationship between changes in the biochemical composition of superficial cutaneous melanomas and their invasive capacity, as well as the possibility of using this relationship in melanoma diagnostics. A comparative pathomorphological, ultrastructural, and spectroscopic study of 128 samples of superficial spreading melanoma removed during radical surgical excision was conducted. A higher frequency and diversity of endogenous pigment analytes were detected during the horizontal phase of tumor growth compared to the vertical phase. Diagnostically significant analytes included carotenoid pigments ($p=0.02257$), porphyrin ($p=0.09080$), and melanin precursors tyrosine ($p=0.01554$) and phenylalanine ($p=0.01753$). The use of a comprehensive pathomorphological and spectroscopic study and multiplex analysis of the obtained results made it possible to simultaneously identify a significant number of statistically confirmed endogenous pigment analytes in superficial melanoma skin samples. These analytes have diagnostic value in assessing the invasive capacity of superficial melanomas.

Key words: superficial melanoma of the skin, endogenous pigment, analyte, melanin, carotenoid, porphyrin, invasive capacity.

Contacts: Nichiporov A.I., e-mail: andrei.ni4iporov@yandex.ru

For citations: Borisov A.V., Chernov I.A., Avdalyan A.M., Timofeev S.E., Ronzin A.V., Nichiporov A.I., Kukushkin V.I., Kirillov Yu.A. Use of endogenous pigment analytes to assess the invasive potential of superficial skin melanomas, *Biomedical Photonics*, 2026, vol. 15, no. 1, pp. 4–10. doi: 10.24931/2413–9432–2026–15-1-4-10

ИСПОЛЬЗОВАНИЕ АНАЛИТОВ ЭНДОГЕННЫХ ПИГМЕНТОВ ДЛЯ ОЦЕНКИ СПОСОБНОСТИ К ИНВАЗИИ ПОВЕРХНОСТНЫХ МЕЛАНОМ КОЖИ

А.В. Борисов[1], И.А. Чернов[1], А.М. Авдалян[2], С.Е. Тимофеев[2], А.В. Ронзин[2], А.И. Ничипоров[2], В.И. Кукушкин[3], Ю.А. Кириллов[1,2,4]
[1]Тюменский государственный медицинский университет, Тюмень, Россия
[2]Московский многопрофильный клинический центр «Коммунарка», Москва, Россия
[3]Институт физики твёрдого тела Российской академии наук, Черноголовка, Россия
[4]Российский научный центр хирургии имени академика Б.В. Петровского, Москва, Россия

Резюме

Меланома кожи, на долю которой приходится 70-80% всех диагностируемых опухолей, развивающихся из меланинобразующей ткани, представляет собой пример злокачественной опухоли, инициация и развитие которой за редким исключением сопряжены с реализацией эндогенных пигментаций в морфологическом субстрате опухоли. Вместе с тем, существующая диагностическая парадигма поверхностных меланом кожи не учитывает значение эндогенных пигментаций для оценки способности опухоли к инвазии. Настоящая статья посвящена исследованию связи между изменениями в биохимическом составе поверхностных меланом кожи и их способности к инвазии, а также возможности использования этой связи при проведении диагностики меланомы. Было проведено

сравнительное патоморфологическое, ультраструктурное и спектроскопическое исследование 128 образцов поверхностно распространяющейся меланомы, удаленных во время радикального хирургического иссечения. Выявлена большая частота и разнообразие аналитов эндогенных пигментов в горизонтальную фазу роста опухоли по сравнению с вертикальной. К диагностически значимым аналитам отнесены пигменты каротиноиды (p=0,02257), порфирин (p=0,09080), а также предшественники меланина тирозин (p=0,01554) и фенилаланин (p=0,01753). Использование комплексного патоморфологического и спектроскопического исследования и мультиплексный анализ полученных результатов позволили идентифицировать в образцах поверхностной меланомы кожи одновременно значительное количество подтверждённых статистически аналитов эндогенных пигментов, имеющих диагностическое значение в оценке способности поверхностных меланом кожи к инвазии.

Ключевые слова: поверхностная меланома кожи, аналит, эндогенный пигмент, меланин, каротиноид, порфирин, способность к инвазии.

Контакты: Ничипоров А.И., e-mail: andrei.ni4iporov@yandex.ru

Для цитирования: Борисов А.В., Чернов И.А., Авдалян А.М., Тимофеев С.Е., Ронзин А.В., Ничипоров А.И., Кукушкин В.И., Кириллов Ю.А. Использование аналитов эндогенных пигментов для оценки способности к инвазии поверхностных меланом кожи // Biomedical Photonics. – 2026. –Т. 15, № 1. – С. 4–10. doi: 10.24931/2413–9432–2026–15-1-4-10

Introduction

The results of numerous studies on the epidemiology of oncological diseases convincingly demonstrate an increase in morbidity and mortality rates in the vast majority of countries worldwide [1,2]. All this fully applies to cutaneous melanoma, which accounts for over 70% [3] of all diagnosed tumors developing from melanin-producing tissue. The progress observed in recent years in the early and effective diagnosis of melanoma is due to the use of precision immunohistochemical and molecular genetic research methods [4,5]. The diagnostic paradigm for cutaneous melanoma remains relatively conservative and does not take into account the importance of endogenous pigmentations found in the tumor tissue substrate, which play a key role in determining its invasive potential.

Materials and Methods

We studied 128 samples of superficial spreading melanoma removed during radical surgical excision and submitted for pathohistological examination in accordance with Order No. 179n of the Russian Ministry of Health dated March 24, 2016, "On the Rules for Conducting Pathological and Anatomical Studies." The first group (n = 83) included superficial melanoma samples with a predominantly horizontal growth phase, often with features of Pagetoid melanoma. The second group (n = 45) included samples with a predominantly vertical growth phase. The control group (n = 10) consisted of facial skin samples (autopsy material) with no clinical or morphological manifestations of skin pathology. Skin samples were fixed for 24-48 hours in 10% neutral formalin in a phosphate buffer (pH 7.4). Skin processing was performed automatically using a Pathos Delta processor (Milestone, Italy), and paraffin embedding was performed using a Leica HistoCore (Leica, Germany). Serial 3-4 µm-thick sections, prepared on a ThermoFisherScientific HM 325 microtome (USA), were stained with hematoxylin and eosin, picrofuchsin according to van Gieson, and according to Mallory. Melanin was detected by silvering using the Fontana-Masson method. Skin samples directly adjacent to the melanoma and visually unchanged were examined under an electron microscope. Skin fragments, 1 mm^3 in volume, were fixed in a 2.5% glutaraldehyde solution in collidine buffer (pH 7.4) at room temperature for 1.5 h, and post-fixed in a 1% osmium tetroxide solution for 1.0-1.5 h at +4–+6^0 C. The material was dehydrated in alcohols of increasing concentration (from 50^0 to 96^0) and several portions of ether, and embedded in Araldite. Semi-thin sections were stained with methylene blue, and ultra-thin sections were contrasted with uranyl acetate and lead citrate [6].

Tissue structure was visualized in ultrathin sections using a Zeiss EVO LS10 scanning electron microscope (Zeiss, Germany) with a STEM detector.

Spectroscopic examination of the biological samples was also performed using an InSpektr M spectrometer, version M-532 (RU dated June 18, 2021, No. RZN 2015/2419, manufacturer: RamMix LLC, Russia), consisting of an Olympus CX41 optical microscope and a spectrometer unit with an excitation wavelength of 532 nm. The laser spot diameter at the focal point was 10 µm, and the laser power was 10 mW. Instrument control, spectral recording, and spectral acquisition were performed using the specialized InSpektr software, also developed by RamMix LLC (Chernogolovka). The program identified chemical substances and recorded changes in their quantitative and qualitative composition in the biological sample under study using spectra combining Raman and fluorescence signals. The spectra of biological molecules identified during the study were assigned to the corresponding substance class and displayed as separate columns or fields in the database. Their detection or absence was reflected as a binary indicator (yes/no). Raman spectroscopy was used to

identify both certain pigments (porphyrin, carotenoids) and analyte components related to melanin pigment precursors (tyrosine, phenylalanine) (Table 1).

To compare the identified changes, the results of studies of control skin tissue samples obtained from individuals without skin pathology were used. Database creation and subsequent statistical processing were performed using specialized software: R-4.3.0 (The R Foundation, Austria) and RStudio Desktop (Version 2023.06.1, RStudio Inc, USA). Additional R packages within this software were used for descriptive statistics, building regression models, and data visualization.

Statistical significance of differences was assessed at a significance level of $p < 0.05$.

The study protocol was reviewed and approved by the Ethics Committees of the State Budgetary Healthcare Institution "Moscow Multidisciplinary Clinical Center "Kommunarka" of the Moscow Department of Health (extract from protocol No. 6 dated August 8, 2023) and the Federal State Budgetary Educational Institution "Tyumen State Medical University" of the Ministry of Health of the Russian Federation (extract from protocol No. 121 dated May 22, 2024).

Results and Discussion

Macroscopically, all melanomas examined exhibited at least three of the five ABCDE features [7] (Fig. 1*a*) and were confirmed dermoscopically (Fig. 1*b*). In the first group of samples (n = 83), the tumor was localized in the dermatoepidermal junction, epidermis, and partially in the papillary dermis (Fig. 1*cd*).

Atypical melanocytes could be located singly (Fig. 2*a*) or formed tumor clusters, which was expectedly accompanied by the development of intercellular

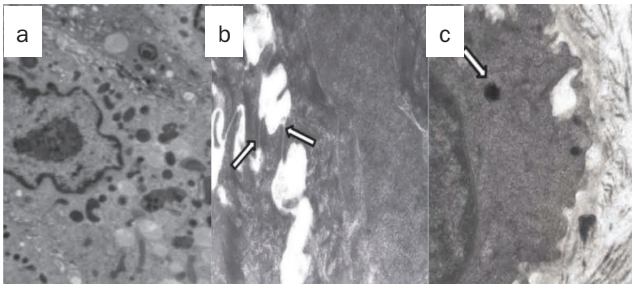

Рис. 2. Ультраструктурные особенности клеточной составляющей поверхностной меланомы кожи:
a – атипизм ультраструктур меланоцита опухоли, нарушение ядерно-цитоплазматического отношения, гетерогенность меланосом. Трансмиссионная электронная микроскопия х 9000;
b – включения меланина и межклеточный отёк (спонгиоз) между базальным и шиповатым слоями эпидермиса. Десмосома – белая стрелка. Трансмиссионная электронная микроскопия х 11000;
c – липофусцин в цитоплазме кератиноцита базального слоя эпидермиса - белая стрелка. Трансмиссионная электронная микроскопия х 12000.
Fig. 2. Ultrastructural features of the cellular component of superficial skin melanoma:
a – atypia of tumor melanocyte ultrastructures, violation of the nuclear-cytoplasmic ratio, heterogeneity of melanosomes. Transmission electron microscopy x 9000;
b – inclusions of melanin and intercellular edema (spongiosis) between the basal and spinous layers of the epidermis. Desmosome - white arrow. Transmission electron microscopy x 11000;
c – lipofuscin in the cytoplasm of the keratinocyte of the basal layer of the epidermis - white arrow. Transmission electron microscopy x 12000.

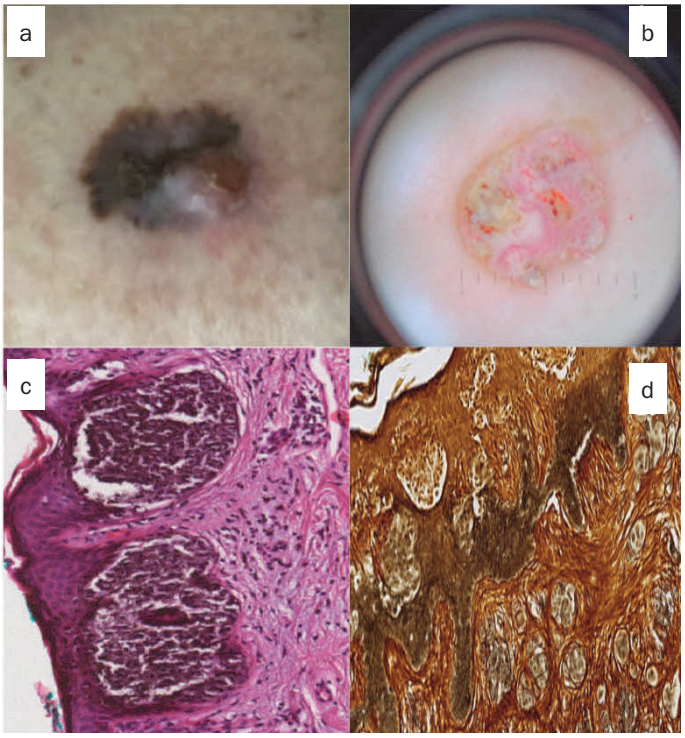

Рис. 1. Поверхностно-распространяющаяся меланома кожи туловища:
a – неравномерности границ новообразования и распределения пигмента, цветовое разнообразие в отсутствие выраженной асимметрии и возвышения;
b – фотофиксация изображения новообразования, полученного при помощи дерматоскопа;
c – педжетоидная поверхностная меланома, атипичные меланоциты и формируемые ими комплексы в области дерматоэпидермального абриса, эпидермисе и частично сосочковом слое дермы. Окраска гематоксилином и эозином х 150;
d – скопления меланина в эпидермисе и дерме. Серебрение по Фонтана-Массону х 70.
Fig. 1. Superficial spreading melanoma of the skin of the trunk:
a – uneven boundaries of the neoplasm and distribution of pigment, color diversity in the absence of pronounced asymmetry and elevation;
b – photographic recording of an image of a neoplasm obtained using a dermatoscope;
c – pagetoid superficial melanoma: atypical melanocytes and the complexes they form in the area of the dermatoepidermal outline, epidermis and partially the papillary layer of the dermis. Hematoxylin and eosin staining x 150;
d – accumulations of melanin in the epidermis and dermis. Silvering according to Fontana-Masson x 70.

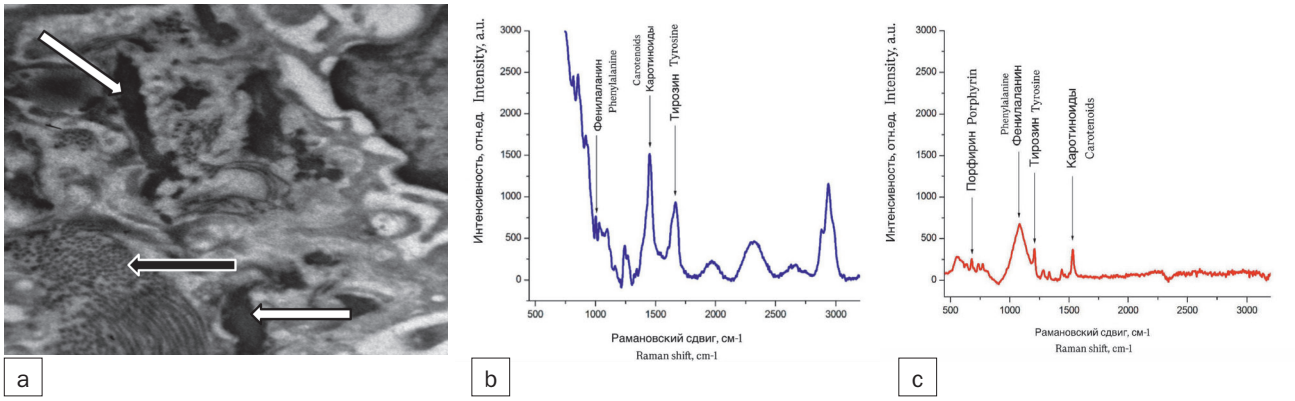

Рис. 3. Поверхностно-распространяющаяся меланома кожи со спектральными образцами горизонтальной и вертикальной фаз роста:
a – игольчатые отложения порфирина (белые стрелки) и коллаген (черная стрелка) в субэпидермальном пространстве дермы. Трансмиссионная электронная микроскопия х 12000;
b – спектральная характеристика меланомы в фазу горизонтального роста (пояснения в тексте);
c – спектральная характеристика меланомы в фазу вертикального роста (пояснения в тексте).
Fig. 3. Superficial spreading melanoma of the skin with spectral patterns of horizontal and vertical growth phases:
a – needle-like deposits of porphyrin (white arrows) and collagen (black arrow) in the subepidermal space of the dermis. Transmission electron microscope x 12000;
b – spectral characteristics of melanoma in the horizontal growth phase (explanations in the text);
c – spectral characteristics of melanoma in the vertical growth phase (explanations in the text).

edema in the spinous layer of the epidermis (Fig. 2*b*). Keratinocytes in the basal layer of the epidermis often contained small lipofuscin inclusions (Fig. 2c), which differed from melanin grains by their ultrastructural heterogeneity and lower electron density.

Porphyrin accumulations in the form of needle-like formations were localized predominantly in the dermatoepidermal junction and dermis (Fig. 3a). In samples from the second group (n = 45), tumor complexes and individual atypical melanocytes were localized in the papillary and reticular layers of the dermis. Tumors with a vertical growth phase were characterized by higher rates of invasion, tumor substrate thickness, mitosis, and the frequency of both pigments and their precursors compared to those in the first group (Table 1). The spectra of the control group skin samples were characterized by high initial fluorescence values and an abundance of both non-specific and specific identifiable analytes, including melanin precursors (phenylalanine and tyrosine) with a distribution of molecular vibration intensities of phenylalanine at 1003.8 cm^{-1} and 1045.1 cm^{-1}, and tyrosine at 1172.4 cm^{-1}. In comparison, the spectra of skin samples with superficially spreading melanoma in the horizontal growth phase showed higher total initial fluorescence (from 3000 arbitrary units) and a diverse composition of specific, so-called "pigment" analytes, with molecular vibration intensities at 1002 cm^{-1} (phenylalanine), 1614.4 cm^{-1} (tyrosine), 1122 cm^{-1} (porphyrin), and 1480 cm^{-1} (carotenoids) (Fig. 3*b*).

The initiation and development of the vertical phase of melanoma growth in the spectra were accompanied by low values of the initial fluorescence of biological objects, minimal differences between the initial, maximum, and residual fluorescence values, and the presence of Raman peaks of analytes of precursors of proteinogenic chromoproteins (Fig. 3*c*).

To statistically evaluate the relationship between each of the two tumor growth phases and the analytes detected in it by Raman spectroscopy, binary logistic regression was used as a statistical analysis method. In this model, the dependent or studied variable was the tumor growth phase, and the independent variables were the analytes detected during spectroscopy [8, 9]. Two working hypotheses were formulated. The first, designated as H_0, assumed the absence of differences in the frequencies of determination of tyrosine, phenylalanine, porphyrin and carotenoids between the horizontal and vertical phases of tumor growth. The alternative hypothesis H_1 assumed the presence of statistically significant differences between the tumor growth phases and the identified analytes. The obtained results demonstrated the statistical significance of carotenoids ($p = 0.02257$), tyrosine ($p = 0.01554$) and phenylalanine ($p = 0.01753$) (Table 2).

It should be noted that each coefficient in the resulting model represents the logarithmic odds ratio of transition to the vertical growth phase for each unit increase in the corresponding analyte value, holding all other variables constant. Carotenoids, tyrosine, and phenylalanine have a negative effect on the probability of transition to the vertical growth phase of superficial spreading melanoma, as their estimated values are less than zero. This means that detection of these components by Raman spectroscopy increases the probability of a tumor being in the horizontal growth phase.

Таблица 1
Выявленные при рамановской спектроскопии пигменты и их предшественники в различные фазы роста поверхностно-распространяющихся меланом кожи

Table 1
Pigments and their precursors identified by Raman spectroscopy in different growth phases of superficial spreading melanomas of the skin

№	Признак / Characteristic	Количество, % / Count, %
1	Фазы роста опухоли / The phase of tumor growth	128 (100%)
	Радиальная / Horizontal	83 (64,8%)
	Вертикальная / Vertical	45 (35,2%)
2	Компоненты, выявленные при помощи рамановской спектроскопии/ Raman Spectroscopy-detected biomarkers	
	Тирозин / Tyrosine	86/128 (67,2%)
	Фенилаланин / Phenylalanine	69/128 (53,9%)
	Порфирин / Porphyrin	75/128 (58,6%)
	Каротиноиды / Carotenoids	62/128 (48,4%)
3	Частоты выявления компонентов посредством рамановской спектроскопии в различные фазы роста меланомы / Raman Spectroscopy-based detection rates of biomarkers during melanoma growth phases	
	А) Фаза радиального роста / A) Horizontal growth phase	
	Тирозин / Tyrosine	63/83 (75,9%)
	Фенилаланин / Phenylalanine	54/83 (65,1%)
	Порфирин / Porphyrin	44/83 (53,0%)
	Каротиноиды / Carotenoids	47/83 (56,6%)
	Б) Фаза вертикального роста / B) Vertical growth phase	
	Тирозин / Tyrosine	23/45 (51,1%)
	Фенилаланин / Phenylalanine	15/45 (33,3%)
	Порфирин / Porphyrin	31/45 (68,9%)
	Каротиноиды / Carotenoids	15/45 (33,3%)

Таблица 2
Результаты расчета коэффициентов, включенных в модель бинарной логистической регрессии

Table 2
Results of calculating the coefficients included in the binary logistic regression model

Коэффициенты / Coefficients	Оценка / Value	Стандартная ошибка / Standart mistake	Уровень значимости p / Significance level of p
Intercept (свободный член) / Intercept (free member)	1,3934	0,5923	0,01865*
Каротиноиды / Carotenoids	-1,0158	0,4454	0,02257*
Порфирин / Porphyrin	0,7829	0,4629	0,09080
Тирозин / Tyrosine	-1,1103	0,4589	0,01554*
Фенилаланин / Phenylalanine	-1,0596	0,4461	0,01753*

*статистически значимые показатели аналитов фазы роста меланомы
*statistically significant indicators of melanoma growth phase analyte values

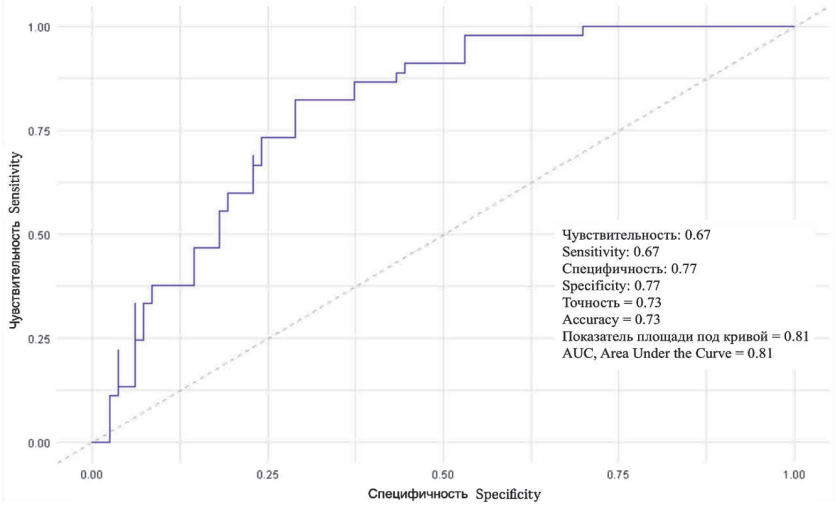

Рис. 4. ROC-анализ оценки модели перехода меланомы кожи в вертикальную фазу роста.
Fig. 4. ROC-analysis for assessing the model of cutaneous melanoma transition to vertical growth phase.

The quality of the binary classification was assessed using a Receiver Operating Characteristic (ROC) curve (Fig. 4). The area under the curve (AUC) was 0.81, indicating the good ability of the model to differentiate tumor growth phases. The specificity of model was 0.77, sensitivity was 0.67, and the proportion of correctly classified cases among all examples (accuracy) reached 0.73.

Based on the obtained results, a model for predicting the vertical growth phase of superficial spreading melanomas based on Raman spectroscopy data is presented as follows:

$$p=\frac{1}{1+e^{-(1.3934-1.0158\times Carotenoids+0.7829\times Porphyrin-1.1103\times Tyrosine-1.0596\times Phenylalanine)}}$$

where:

- p is the probability that the melanoma is in the vertical growth phase
- e is the base of the natural logarithm ≈ 2.718

If $p>0.5$, the model predicts a vertical growth phase; if $p<0.5$, it indicates a horizontal growth phase.

It should be noted that, despite the obtained significance level for porphyrin being $p = 0.09080$, which exceeds the established one for this study, we considered it necessary to include it in the prognostic model. This decision is based on data from reputable scientific sources indicating a high concentration of porphyrins in malignant tumors [10-12]. The lower number of melanoma cases in the vertical growth phase observed in our study compared to the horizontal phase may explain the lack of statistical significance of porphyrin and does not allow to confidently exclude it from the model.

Conclusion

Despite significant advances in the diagnosis and therapy of melanomas, treatment of these tumors remains a challenge, as the stability of positive results is not always achieved. The need to update existing diagnostic criteria became evident after the publication of R. Virchow's seminal work on oncology [13]. Over the years, this approach has been repeatedly revised due to the introduction of highly accurate diagnostic methods. Today, medical science seeks to understand the nature of melanoma precisely through the lens of its metabolic features, suggesting that it is the metabolic products, including pigments, that may serve as potential diagnostic markers [14–15]. The present study aims to assess the importance of endogenous pigmentation in identifying the invasiveness of cutaneous melanoma.

REFERENCES

1. Shakhzadova A.O., Starinsky V.V., Lisichnikova I.V. The state of cancer care for the population of Russia in 2022. *Siberian Journal of Oncology,* 2023, Vol. 22 (5), pp. 5-13. doi:10.21294/1814-4861-2023-22-5-5-13
2. Siegel R.L., Miller K.D., Jemal A. Cancer statistics. *A Cancer Journal for Clinicians,* 2020, Vol. 70(1), pp. 7-30. doi:10.3322/caac.21590.
3. Ostrowski S.M., Fisher D.E. Biology of melanoma. *Hematology/Oncology Clinics of North America,* 2021, Vol. 35(1), pp. 29-56. doi:10.1016/j.hoc.2020.08.010.
4. Namikawa K., Yamazaki N. Targeted Therapy and Immunotherapy for Melanoma in Japan. *Current Treatment Options in Oncology,* 2019, Vol. 20(1). doi:10.1007/s11864-019-0607-8.

ЛИТЕРАТУРА

1. Shakhzadova A.O., Starinsky V.V., Lisichnikova I.V. The state of cancer care for the population of Russia in 2022 // Siberian Journal of Oncology – 2023. – Vol. 22, №. 5 – P. 5-13. doi:10.21294/1814-4861-2023-22-5-5-13
2. Siegel R.L., Miller K.D., Jemal A. Cancer statistics // A Cancer Journal for Clinicians – 2020. – Vol. 70, № 1 – P. 7-30. doi:10.3322/caac.21590.
3. Ostrowski S.M., Fisher D.E. Biology of melanoma // Hematology/Oncology Clinics of North America – 2021. – Vol. 35, № 1 – P. 29–56. doi:10.1016/j.hoc.2020.08.010.
4. Namikawa K., Yamazaki N. Targeted Therapy and Immunotherapy for Melanoma in Japan // Current Treatment Options in Oncology – 2019. – Vol. 20, № 1. doi:10.1007/s11864-019-0607-8.

5. Mao L., Qi Z., Zhang L., Guo J., Si L. Immunotherapy in Acral and Mucosal Melanoma: Current Status and Future Directions. *Frontiers in immunology,* 2021, Vol. 12, pp. 1-13. doi:10.3389/fimmu.2021.680407.eCollection 2021.
6. Reynolds E.S. The use of lead citrate at high pH as an electron-opaque stain in electron microscopy. *Journal of Cell Biology,* 1963, Vol. 17(1), pp. 208-212. doi:10.1083/jcb.17.1.208
7. Friedman R.J., Rigel D.S., Kopf A.W. Early detection of malignant melanoma: the role of physician examination and self-examination of the skin. *A Cancer Journal for Clinicians,* 1985, Vol. 35(3), pp. 130-151. doi:10.3322/canjclin.35.3.130.
8. Pavri S.N., Clune J., Ariyan S., Narayan D. Malignant Melanoma: Beyond the Basics.*PlastReconstrSurg,* 2016, Vol. 138(2), pp. 330-340. doi:10.1097/PRS.0000000000002367.
9. Bobos M. Histopathologic classification and prognostic factors of melanoma: a 2021 update. *Italian Journal of Dermatology and Venereology,* 2021, Vol. 156, no. 3, pp. 300-321. doi:10.23736/S2784-8671.21.06958-3.
10. Tsolekile N., Nelana S., Oluwafemi O.S. Porphyrin as Diagnostic and Therapeutic Agent. *Molecules,* 2019, Vol. 24(14), pp. 2669 doi:10.3390/molecules24142669.
11. Nishida K., Tojo T., Kondo T., Yuasa M. Evaluation of the correlation between porphyrin accumulation in cancer cells and functional positions for application as a drug carrier. *Scientific Reports,* 2021, Vol. 11(1), pp. 2046. doi:10.1038/s41598-021-81725-3.
12. Yang F., Xu M., Chen X., Luo Y. Spotlight on porphyrins: Classifications, mechanisms and medical applications. *Biomedicine & Pharmacotherapy,* 2023, vol. 164, pp. 114933. doi:10.1016/j.biopha.2023.114933.
13. Virchow R. Die krankheiten Geschwiulste. *Course taught at the University of Berlin* , 1863, Vol. 24, pp. 369-434.
14. Medori M.C., Donato K., Dhuli K., Maltese P.E., Tanzi B., Tezzele S., Mareso C., Miertus J., Generali D. et al. Omics sciences and precision medicine in melanoma. *Clinica terapeutica,* 2023, Vol. 174, suppl. 2(6), pp. 29-36. doi:10.7417/CT.2023.2469.
15. Routy B., Jackson T., Mählmann L., Baumgartner C.K., Blaser M., Byrd A., Corvaia N., Couts K., Davar D., Derosa L. et al. Melanoma and microbiota: Current understanding and future directions. *Cancer*

5. Mao L., Qi Z., Zhang L., Guo J., Si L. Immunotherapy in Acral and Mucosal Melanoma: Current Status and Future Directions // Frontiers in immunology – 2021. – Vol. 12 – P. 1-13. doi:10.3389/fimmu.2021.680407.
6. Reynolds E.S. The use of lead citrate at high pH as an electron-opaque stain in electron microscopy // Journal of Cell Biology – 1963. – Vol. 17, № 1 – P. 208-212. doi:10.1083/jcb.17.1.208
7. Friedman R.J., Rigel D.S., Kopf A.W. Early detection of malignant melanoma: the role of physician examination and self-examination of the skin // A Cancer Journal for Clinicians – 1985. – Vol. 35, № 3 – P. 130–151. doi:10.3322/canjclin.35.3.130.
8. Pavri S.N., Clune J., Ariyan S., Narayan D. Malignant Melanoma: Beyond the Basics // Plast Reconstr Surg – 2016. – Vol. 138, № 2 – P. 330-340. doi:10.1097/PRS.0000000000002367.
9. Bobos M. Histopathologic classification and prognostic factors of melanoma: a 2021 update // Italian Journal of Dermatology and Venereology – 2021. – Vol. 156, № 3 – P. 300-321. doi:10.23736/S2784-8671.21.06958-3.
10. Tsolekile N., Nelana S., Oluwafemi O.S. Porphyrin as Diagnostic and Therapeutic Agent // Molecules – 2019. – Vol. 24, № 14 – P. 2669 doi:10.3390/molecules24142669.
11. Nishida K., Tojo T., Kondo T., Yuasa M. Evaluation of the correlation between porphyrin accumulation in cancer cells and functional positions for application as a drug carrier // Scientific Reports – 2021. – Vol. 11, № 1 – P. 2046. doi:10.1038/s41598-021-81725-3.
12. Yang F., Xu M., Chen X., Luo Y. Spotlight on porphyrins: Classifications, mechanisms and medical applications // Biomedicine & Pharmacotherapy – 2023. – Vol. 164 – P. 114933. doi:10.1016/j.biopha.2023.114933.
13. Virchow R. Die krankheiten Geschwiulste // Course taught at the University of Berlin – 1863. – Vol. 24: P. 369-434.
14. Medori M.C., Donato K., Dhuli K., Maltese P.E., Tanzi B., Tezzele S., Mareso C., Miertus J., Generali D. et al. Omics sciences and precision medicine in melanoma // Clinica terapeutica – 2023. – Vol. 174, Suppl. 2, № 6 – P. 29-36. doi:10.7417/CT.2023.2469.
15. Routy B., Jackson T., Mählmann L., Baumgartner C.K., Blaser M., Byrd A., Corvaia N., Couts K., Davar D., Derosa L. et al. Melanoma and microbiota: Current understanding and future directions // Cancer Cell – 2024. – Vol. 42, № 1 – P. 16-34. doi:10.1016/j.ccell.2023.12.003.

PHOTOBIOMODULATION OF ACUTE PAIN SYNDROME AFTER COMPLEX TOOTH EXTRACTION

Yudin D.K.[1], Kastyro I.V.[1], Romanko Yu.S.[2], Ali R.B.[1], Popadyuk V.I.[1], Zaborova V.A.[2], Dragunova S.G.[1], Gusev K.S.[1]
[1]Peoples' Friendship University of Russia (RUDN University), Moscow, Russia
[2]Sechenov First Moscow State Medical University (Sechenov University), Moscow, Russia

Abstract

The study evaluated various types of low-intensity photobiomodulatory therapy (PBMT) in reducing acute pain after complex tooth extraction. Complex extraction of maxillary molars and premolars (no more than two teeth, on one side) was performed in 119 patients (aged 18-44 years). In Group 1 (n = 28), PBMT was not performed. In Group 2 (n = 32), pulsed infrared laser radiation in combination with a magnetic mirror tip was used. In Group 3 (n = 30), dental tips with a pulsed infrared laser emitting head were used in the area of the socket formed after tooth extraction. In Group 4 (n = 29), a laser head with a continuous red spectrum was used. The exposure time of the tips and heads in all groups was 3 minutes in the projection of the extracted tooth. All patients underwent PBMT at 1, 24, and 48 hours after surgery. At these same times, acute pain was assessed using a visual analog scale (VAS) and a numerical rating scale (NRS) in millimeters. Acute pain was lowest already on the first postoperative day in the pulsed infrared laser group with a mirror magnetic head. Among the PBMT groups, the continuous red laser demonstrated the worst pain results. In the group without PBMT, pain requiring medical management persisted for up to 48-72 hours after tooth extraction.

Key words: photobiomodulating therapy, tooth extraction, pain syndrome, visual analogue scale, digital rating scale.

Contacts: Kastyro I.V., e-mail: ykastyro@gmail.com

For citations: Yudin D.K., Kastyro I.V., Romanko Yu.S., Ali R.B., Popadyuk V.I., Zaborova V.A., Dragunova S.G., Gusev K.S. Photobiomodulation of acute pain syndrome after complex tooth extraction, *Biomedical Photonics*, 2026, vol. 15, no. 1, pp. 11–18. doi: 10.24931/2413–9432–2026–15-1-11-18

ФОТОБИОМОДУЛЯЦИЯ ОСТРОГО БОЛЕВОГО СИНДРОМА ПОСЛЕ СЛОЖНОГО УДАЛЕНИЯ ЗУБА

Д.К. Юдин[1], И.В. Кастыро[1], Ю.С. Романко[2], Р.Б. Али[1], В.И. Попадюк[1], В.А. Заборова[2], С.Г. Драгунова[1], К.С. Гусев[1]
[1]ФГАОУ ВО Российский Университет дружбы народов имени Патриса Лумумбы, Москва, Россия
[2]Первый Московский государственный медицинский университет им. И.М. Сеченова, Москва, Россия

Резюме

В исследовании были оценены различные виды воздействия низкоинтенсивной фотобиомодулирующей терапии (ФБМТ) на снижение острого болевого синдрома после сложного удаления зуба. Сложное удаление моляров и премоляров верхней челюсти (не более двух зубов и с одной стороны) было проведено у 119 пациентов (возраст 18-44 года). В 1-й группе (n = 28) не проводили ФБМТ. Во 2-й группе (n = 32) применяли импульсное инфракрасное лазерное излучение в сочетании с магнитной зеркальной насадкой. В 3-й группе (n = 30) применяли стоматологические насадки с импульсной инфракрасной лазерной излучающей головкой в области, сформированной после удаления зуба лунки. В 4-й группе (n = 29) использоваи лазерную головку с непрерывным красным спектром. Время экспозиции насадок и головок во всех группах составляло 3 мин в проекции удаленного зуба. Всем пациентам ФБМТ проводили через 1, 24 и 48 ч после хирургического вмешательства и в эти же сроки оценивали острый болевой синдром при помощи визуально-аналоговой шкалы (ВАШ) и цифровой рейтинговой шкалы (ЦРШ) в мм. Острый болевой синдром был самым низким уже в первые постоперационные сутки в группе импульсного инфракрасного лазерного излучения с зеркальной магнитной головкой. Среди групп

с ФБМТ худший результат по уровню боли был показан при применении непрерывного красного лазера. В группе без ФБМТ боль, требующая медикаментозной коррекции, сохранялась до 48-72 ч после удаления зуба.

Ключевые слова: фотобиомодулирующая терапия, удаление зуба, болевой синдром, визуально-аналоговая шкала, цифровая рейтинговая шкала.

Контакты: Кастыро И.В., e-mail: ykastyro@gmail.com

Для цитирования: Юдин Д.К., Кастыро И.В., Романко Ю.С., Али Р.Б., Попадюк В.И., Заборова В.А., Драгунова С.Г., Гусев К.С. Фотобиомодуляция острого болевого синдрома после сложного удаления зуба // Biomedical Photonics. – 2026. –Т. 15, № 1. – С. 11–18. doi: 10.24931/2413–9432–2026–15-1-11-18

Introduction

Tooth extraction is a surgical dental procedure that can lead to a number of complications [1]. The histological healing process of sockets after tooth extraction is a four-stage sequential process, including a blood clot phase, an inflammation phase, a proliferation phase, and a modeling and remodeling phase [2, 3]. Following tooth extraction, a blood clot begins to form within the first minutes, performing a protective function and serving as a matrix for further thrombus formation and subsequent healing. During the inflammation phase, immune-inflammatory reactions are triggered, accompanied by the formation of granulation tissue, which is critical for wound cleansing of necrotic tissue and creating conditions for healing [1, 4, 5]. Early in this stage, acute postoperative pain syndrome develops [6, 7]. During the recovery phase, active proliferation of bone cells, particularly osteoblasts, and the formation of a trabecular bone structure are observed, which is completed within 4 to 8 weeks after tooth extraction [8]. During the modeling and remodeling stage, bone tissue maturation and remodeling continue, ensuring the mechanical strength and stability of the alveolar ridge. These stages are key to successful healing and tissue restoration after dental interventions, and understanding these processes facilitates the development of effective treatment and rehabilitation methods [9].

The search for new methods to accelerate wound healing after tooth extraction and improve bone restoration is driven by the need for subsequent dental implantation [10, 11]. The use of low-intensity photobiomodulatory therapy (PBMT) allows for the development of new methods for patient rehabilitation during dental surgery [12]. The use of low-intensity PBMT in dental practice helps to reduce inflammatory reactions, has an antibacterial effect, prevents the development of pain, and promotes accelerated tissue healing in the area of damage due to its immune-correcting effect [13].

The aim of the study was to evaluate various options for the effect of low-intensity PBMT on reducing the intensity of acute pain after complex tooth extraction.

Materials and Methods

All patients were divided into 4 groups. Group 1 included 28 patients (7 women and 21 men) aged 18 to 46 years. These patients underwent complex maxillary molar extractions without the use of PBMT. Group 2 included 32 patients (10 women and 22 men) aged 20 to 47 years. PBMT was performed in Group 2 using a LO-904-25 cutaneous laser emitting head with a wavelength of 904 nm and a ZM-50 magnetic mirror attachment with a wavelength of 0.89 μm and a magnetic field strength of 50 mT. The pulsed radiation power in this group was 10 W, and the radiation frequency was 80 Hz. Group 3 included 30 patients (10 women and 20 men) aged 19 to 43 years. In this group, dental tips from the S-1 set were used for PBMT together with the LO-904-25 laser emitting head with a wavelength of 904 nm. The tips were placed in the oral cavity in the area of the socket formed after tooth extraction. The pulsed radiation power in this group was 7 W, and the radiation frequency was 80 Hz. Group 4 consisted of 17 men and 12 women (29 patients) with complex tooth extraction. For PBMT with continuous radiation, a laser head with a wavelength of 0.63 μm (laser head KLO 635-15) was used, emitting a continuous red spectrum, which has an anti-inflammatory (vascular) effect and stimulates cellular proliferation. The radiation power was 10 mW, the radiation frequency was 635 nm. The exposure time of the tips and heads in all groups was 3 minutes in the projection of the extracted tooth. All patients underwent the procedure 1, 24, 48, and 72 hours after surgery using the LAZMIK-01 device (Russia). All patients were prescribed ketorolac 10 mg orally, 1 tablet 3 times daily, for pain relief and amoxicillin + clavulanic acid, 875 mg + 125 mg, 1 tablet 2 times daily for 6 days, to prevent purulent complications. Complex extraction of maxillary premolars and molars was performed in all patients using mucosal infiltration anesthesia and intraosseous administration of articaine hydrochloride and epinephrine in a 1:200,000 ratio. The study included patients who had no more than two teeth removed from one side of the maxilla.

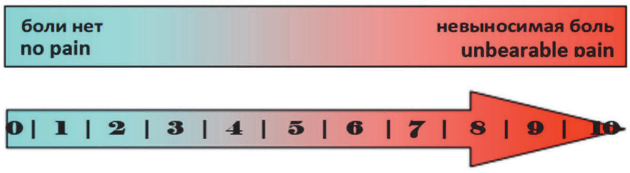

Рис. 1. Визуально-аналоговая шкала (a) и цифровая рейтинговая шкала (b) оценки интенсивности острого болевого синдрома.
Fig. 1. Visual analogue scale (a) and digital rating scale (b) for assessing the intensity of acute pain syndrome.

Pain Assessment

Acute pain was assessed at 1, 3, 24, 48, and 72 hours after complex tooth extraction using a visual analog scale (VAS) (Fig. 1a) and a numerial rating scale (NRS) (Fig. 1b), each 100 mm long. Patients indicated their pain level on the scale using a vertical line at the point on the scale that they believed corresponded to the intensity of their pain. The scales were presented to patients alternately: first the VAS and then the NRS [14]. For each patient, the mean values for both scales were calculated at each pain assessment interval.

Statistical Analysis

Data were processed using Microsoft Excel, MATLAB, STATISTICA 12.6, and JASP 0.14.0.0 software. The Wilcoxon signed-rank test was used to compare data within groups at different times after drug administration. The Kruskal-Wallis, Mann-Whitney, or Student's tests were used to compare data between groups. For each comparison, a significance level was determined based on statistical analysis (from $p < 0.0001$ to 0.05).

According to the Wilcoxon signed-rank test, acute pain, assessed by the mean VAS and NRS scores, was significantly lower in Group 1 at 1 hour postoperatively than at 3 hours ($p < 0.0004$). Pain levels decreased at 24 hours compared to 3 hours postoperatively ($p < 0.007$) and remained unchanged at 48 hours. On the 3rd day, the pain intensity significantly decreased compared to the previous day ($p<0.048$) (Fig. 2a, Table 1). In the 2nd group (pulsed laser therapy with a magnetic mirror attachment), the pain syndrome was significantly higher after 3 hours than after 1 hour after tooth extraction ($p<0.046$). The next day in the 2nd group, the intensity of acute pain significantly decreased compared to the previous point of its assessment ($p<0.042$), and on the 2nd day it decreased significantly again ($p<0.0001$). After another 24 hours (72 hours after the operation), the acute pain syndrome significantly decreased compared to the previous day ($p<0.05$) (Fig. 2b, Table 1). In the 3rd group (the group with pulsed laser therapy), 3 hours after the operation, the pain, as in the other groups, increased ($p<0.029$), and after 3 hours it significantly decreased ($p<0.034$) and continued to decrease significantly on the

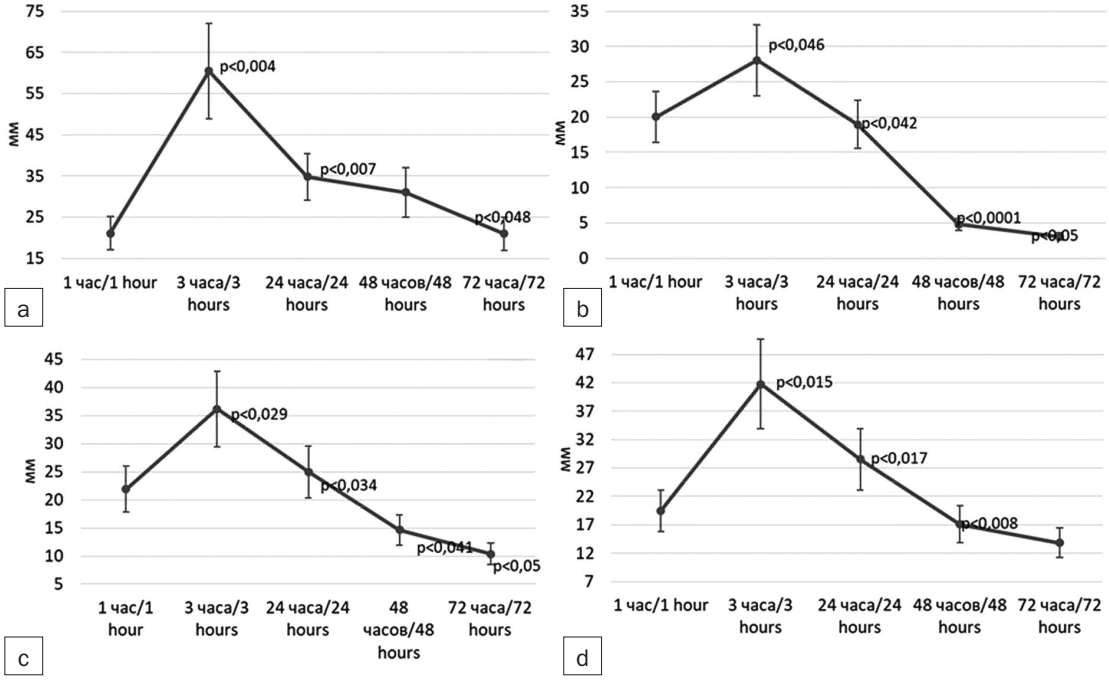

Рис. 2. Внутригрупповая динамика острого послеоперационного болевого синдрома по средним значениям ВАШ и ЦРШ у пациентов со сложным удалением зуба с применением ФБМТ: a – первая группа (группа сравнения); b – вторая группа (группа импульсного лазера+зеркальная магнитная насадка); c – третья группа (группа импульсного лазерного излучения); d – четвертая группа (группа непрерывного лазерного излучения).
Fig. 2. Intragroup dynamics of acute postoperative pain syndrome according to average VAS and NRS values in patients with complex tooth extraction using PBMT: a – first group (comparison group);b – second group (pulsed laser group + mirror magnetic attachment);c – third group (pulsed laser radiation group); d – fourth group (continuous laser radiation group).

2nd ($p<0.041$) and 3rd ($p<0.05$) postoperative days (Fig. 2c, Table 1). Thus, after 3 hours, acute pain significantly increased compared to the 1st postoperative hour ($p<0.015$), and at the 24th ($p<0.017$) and 48th ($p<0.008$) hours it decreased and remained the same at the 72nd postoperative hour of its control (Fig. 2d, Table 1). One hour after complex tooth extraction, no reliable differences were found in all groups of patients. The level of pain syndrome according to the average values of VAS and NRS corresponded to very mild pain.

According to the Mann-Whitney test, the intensity of acute pain in Group 1 3 hours after surgery was significantly higher than in Groups 2, 3, and 4 ($p<0.018$, $p<0.032$, and $p<0.048$, respectively). During this period, patients in Group 2 experienced the least pain compared to the pulsed laser and continuous laser groups ($p<0.045$ and $p<0.048$, respectively).

Twenty-four hours after tooth extraction, the severity of acute pain was significantly lower in Groups 2 ($p<0.012$), 3 ($p<0.036$), and 4 ($p<0.043$) compared to Group 1. Also, as at 3 hours after surgery, in patients of group 2 at the indicated time point, pain intensity was lower than in group 3 ($p < 0.045$) and group 4 ($p < 0.048$) (Fig. 3, Table 1).

Таблица 1
Показатели острой боли по средним значениям ВАШ и ЦРШ после сложного удаления зуба и применения фотобиомодулирующей терапии в раннем послеоперационном периоде

Table 1
Acute pain indices based on average VAS and NRS values after complex tooth extraction and the use of photobiomodulatory therapy in the early postoperative period

мм mm	1 час 1 hour	3 часа 3 hours	24 часа 24 hours	48 часов 48 hours	72 часа 72 hours
1-я группа (сравнения) 1st group (comparisons)	21,05±4,05	60,5±11,64	34,82±5,7	31,03±5,97	20,98±4,03
2-я группа (импульсный лазер+зеркальный магнит) 2nd group (pulse laser + mirror magnet)	20,04±3,6	28,09±5,04	18,96±3,4	4,79±0,86	3,07±0,55
3-я группа (импульсный лазер) 3rd group (pulse laser)	21,91±4,06	36,2±6,72	24,98±4,63	14,66±2,72	10,37±1,92
4-я группа (непрерывный лазер) 4th group (continuous laser)	19,48±3,68	41,75±7,89	28,55±5,39	17,08±3,22	13,84±2,62

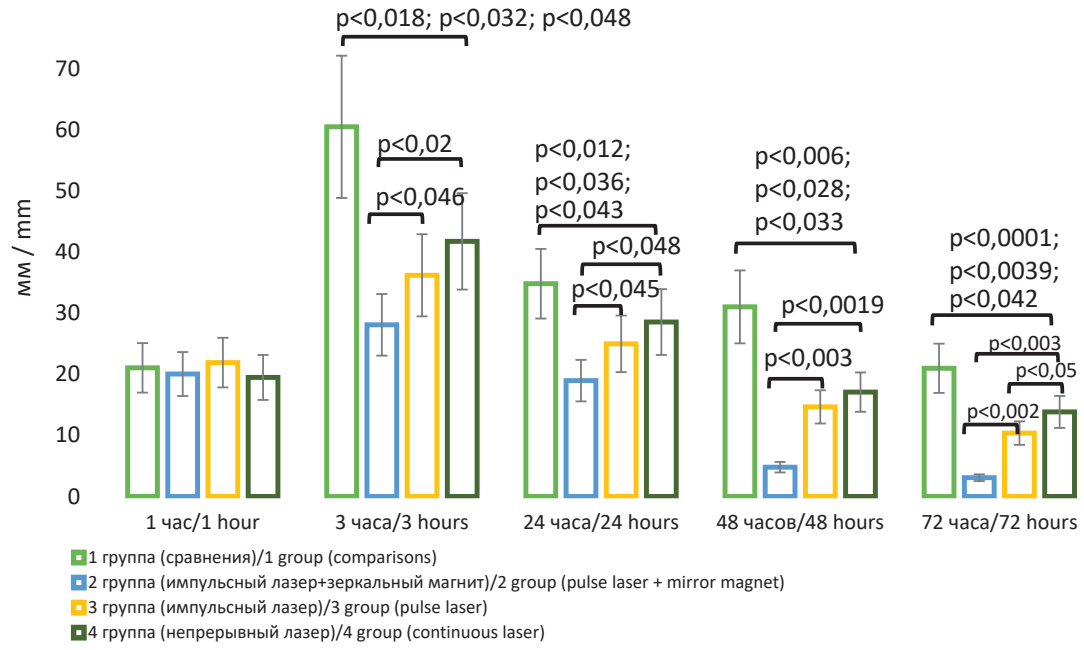

Рис. 3. Динамика острого послеоперационного болевого синдрома по средним значениям ВАШ и ЦРШ у пациентов со сложным удалением зуба с применением ФБМТ.
Fig. 3. Dynamics of acute postoperative pain syndrome according to average values of VAS and NRS in patients with complex tooth extraction using PBMT.

According to the Student's t-test, after 48 hours, pain severity was also higher in Group 1 than in the other PBMT groups (Groups 2, 3, and 4 – $p<0.006$, $p<0.028$, and $p<0.033$, respectively). In group 2, patients experienced practically no pain compared to group 3 ($p < 0.003$) and group 4 ($p < 0.0019$). On the third day (72 hours) after tooth extraction, patients in group 1 experienced significantly higher pain than in the groups with PBMT (groups 2, 3 and 4 - $p < 0.0001$, $p < 0.0039$ and $p < 0.042$, respectively). In group 4, the pain syndrome was significantly higher than in groups 2 ($p < 0.003$) and 3 ($p < 0.05$). Patients in group 2 experienced less intense pain than patients in group 3 ($p < 0.002$) (Fig. 3, Table 1).

Discussion

Healing of dental sockets after tooth extraction is a complex process involving the reconstruction of damaged soft and hard tissues. This process involves the proliferation and differentiation of osteoblasts, as well as the synthesis and mineralization of the extracellular matrix, leading to bone formation and remodeling. New bone formation is regulated by various cytokines, including transforming growth factor β (TGFB), vascular endothelial growth factor (VEGF), insulin-like growth factor (IGF), and bone morphogenetic protein (BMP) [15]. Controlling inflammation and reducing acute pain are particularly important in the early post-extraction period [5, 16-18]. In the study, pain levels were significantly lower in the PBMT groups at all assessment stages compared to patients without PBMT, indirectly indicating the positive anti-inflammatory effects of PBMT combined with nonsteroidal anti-inflammatory drugs (NSAIDs).

An analysis of the use of diode lasers generating radiation in the infrared region of the electromagnetic spectrum demonstrated their bactericidal effect in dental implantation, which can significantly reduce the risk of infectious complications [19]. Low-intensity lasers have been shown to have biostimulating and anti-inflammatory effects, making them useful in wound healing and bone tissue restoration [20, 21]. In the present study, in addition to NSAIDs, antibacterial therapy was also used, but no purulent complications were identified in any of the groups. Nevertheless, the observed pain level clearly indicates the advantage of using PBMT in the early period following complex tooth extraction.

Low-intensity laser irradiation has been shown to promote biostimulation and enhance tissue regenerative potential when applied in doses ranging from 1.5 to 3 J/cm^2. It has been shown that the regenerative properties of the oral epithelium increase, the activity of human gingival fibroblasts changes, and the activity of cells interacting with the implant is modulated, which improves tissue regeneration and reduces the duration of the rehabilitation period in patients [22, 23]. A study by M. Khadra *et al.* demonstrates interesting results regarding the effect of laser therapy on cellular proliferation and the synthesis of important biomolecules. An increase in cell proliferation 96 hours after laser irradiation indicates that laser therapy can activate tissue regeneration and restoration processes. Osteocalcin synthesis, a marker of osteoblastic activity, and TGF-beta (1), a key factor in tissue regeneration and healing, were significantly increased in samples exposed to 3 J/cm^2 laser radiation. This suggests that this therapy may improve implant osseointegration and accelerate bone healing. These results highlight the potential of low-level laser therapy as an effective tool in dentistry and orthopedics. Although, as with any new methods, it is important to continue conducting additional research to confirm and clarify these effects [24]. In the present study, the use of pulsed laser therapy in combination with a mirror magnetic tip resulted in lower pain levels compared to other types of PBMT, which requires clarification of the mechanisms of physiological and pathological changes in tissues depending on the physical characteristics of low-level laser therapy in further clinical and experimental studies.

It has also been established that the use of low-intensity PBMT has a positive effect on the stability of implants 3 weeks after dental implantation [25]. F. Chellini *et al.* evaluated the effect of laser radiation of 808±10 nm average power (2 W, 400 J/cm^2; CW or pulsed mode, 20 kHz, 7 μs, 0.44 W, 88 J/cm^2) on cell viability, their proliferation, adhesion, and also characterized the osteogenic differentiation potential in comparison with the action of chlorhexidine. The authors showed that PBMT has osteoinductive potential, when compared with the cytotoxic effect of chlorhexidine [26]. These data confirm our results, which showed a decrease in the level of acute pain. This indirectly suggests that the type of photobiomodulation applied in the present study helps to reduce inflammation. Reducing inflammatory responses and, consequently, pain levels, leads to improved bone regeneration [27-31].

PBMT improves socket healing during experimental destructive treatment with alendronate in rats. However, pulsed infrared radiation also has a positive effect on the cytoarchitecture of alveolar bone tissue in rats [32]. The present study demonstrated that the higher the PBMT frequency used, the less pain patients reported after complex tooth extraction. These data are consistent with studies evaluating the effectiveness of photobiomodulation after septoplasty. Several studies have shown that in this type of rhinosurgical intervention, which also involves the bony structures of the nasal septum, the use of PBMT leads to a reduction in acute pain in the early postoperative period [33-35]. In previous studies, we have found that low-intensity PBMT not only has a positive local effect, but also reduces the severity of stress reactions, which was demonstrated

in studies of the hippocampus in rats after modeling septoplasty and surgical interventions on the maxilla. Thus, after the use of PBMT in the hippocampus of rats, the level of metabolism of the dopaminergic, noradrenergic and serotonergic systems changes [36]. Moreover, recent studies have shown that during the same experimental surgical interventions, PBMT reduces the level of expression of the stress protein p53, which is responsible for apoptosis, in neurons of the pyramidal layer of the hippocampus [37].

The combined use of PDT and PBMT also promotes more effective tissue restoration after chemoradiotherapy or radiation therapy [38]. Studies of the effectiveness of PBMT demonstrate that increased lipid peroxide and depletion of the antioxidant system are the primary mechanisms of the stress response to various physiological factors. In this process, cell membranes become targets for stress factors, pharmacological agents, and physical agents. PBMT can regulate the formation of free radicals and exert membranotropic effects during PDT of tumors [39, 40].

Conclusion

Although the obtained results indicate the superiority of PBMT over drug therapy alone and the advantage of a pulsed low-intensity infrared laser with a mirror magnetic attachment over a continuous red laser in the management of acute pain after complex tooth extraction, it is necessary to radiographically confirm the effectiveness of these methods in preserving the bone socket and alveolar ridge of the maxilla after complex tooth extraction in clinical practice.

The use of low-intensity PBMT in patients in the early postoperative period following complex tooth extraction results in postoperative pain intensity reductions of 28.2–53.6%, compared to patients without it.

The use of a pulsed low-intensity laser head in combination with a magnetic mirror attachment reduces acute pain in the early postoperative period following complex tooth extraction, compared to the use of a single-pulse emitter and continuous magnetic radiation.

REFERENCES

1. Yang S., Li Y., Liu C., Wu Y., Wan Z., Shen D. Pathogenesis and treatment of wound healing in patients with diabetes after tooth extraction. *Front Endocrinol (Lausanne)*, 2022, Vol. 13, pp. 949535.
2. Zhou S., Li G., Zhou T., Zhang S., Xue H., Geng J., Liu W., Sun Y. The role of IFT140 in early bone healing of tooth extraction sockets. *Oral Dis*, 2022, Vol. 28 (4), pp. 1188-1197.
3. De Sousa Gomes P., Daugela P., Poskevicius L., Mariano L., Fernandes M.H. Molecular and Cellular Aspects of Socket Healing in the Absence and Presence of Graft Materials and Autologous Platelet Concentrates: A Focused Review. *J Oral Maxillofac Res*, 2019, Vol. 10(3). – pp. e2.
4. Dolgalev Al.Al., Svyatoslavov D.S., Pout V.A., Reshetov I.V., Kastyro I.V. Effectiveness of the Sequential Use of Plastic and Titanium Implants for Experimental Replacement of the Mandibular Defect in Animals using Preliminary Digital Design. *Doklady Biochemistry and Biophysics*, 2021, Vol. 496, pp. 36-39.
5. Dragunova S.G., Reshetov I.V., Kosyreva T.F., Severin A.E., Khamidulin G.V., Shmaevsky P.E., A Inozemtsev.N., Popadyuk V.I., Kastyro I.V., Yudin D.K., Yunusov T.Yu., Kleyman V.K., Bagdasaryan V.V., Alieva S.I., Chudov R.V., Kuznetsov N.D., Pinigina I.V., Skopich A.A., Kostyaeva M.G. Comparison of the Effects of Septoplasty and Sinus Lifting Simulation in Rats on Changes in Heart Rate Variability. *Doklady Biochemistry and Biophysics*, 2021, Vol. 498, pp. 165-169.
6. Miroshnychenko A., Ibrahim S., Azab M., Roldan Y., Martinez J.P.D., Tamilselvan D., He L., Little J.W., Urquhart O., Tampi M., Polk D.E., Moore P.A., Hersh E.V., Claytor B., Carrasco-Labra A., Brignardello-Petersen R. Acute Postoperative Pain Due to Dental Extraction in the Adult Population: A Systematic Review and Network Meta-analysis. *J Dent Res*, 2023, Vol. 102 (4), pp. 391-401.
7. Dragunova S., Samoilova M., Ganshin I., Chernolev A. Heart Rate Variability, Pain Syndrome and Cortisol Concentration in Oral Fluid During Sinus-Lifting And Dental Implantation Otorhinolaryngology. *Head and Neck Pathology (ORLHNP)*, 2023, Vol. 2 (4), pp. 31-36.
8. Takahashi S., Kikuchi R., Ambe K., Nakagawa T., Takada S., Ohno T., et al. Lymphangiogenesis and Nos Localization in Healing Process after Tooth Extraction in Akita Mouse. *Bull Tokyo Dent Coll*, 2016, Vol. 57(3), pp. 121-31.
9. Devlin H., Sloan P. Early Bone Healing Events in the Human Extraction Socket. *Int J Oral Maxillofac Surg*, 2002, Vol. 31(6), pp. 641-645.

ЛИТЕРАТУРА

1. Yang S., Li Y., Liu C., Wu Y., Wan Z., Shen D. Pathogenesis and treatment of wound healing in patients with diabetes after tooth extraction // Front Endocrinol (Lausanne). – 2022. – Vol. 13. – P. 949535.
2. Zhou S., Li G., Zhou T., Zhang S., Xue H., Geng J., Liu W., Sun Y. The role of IFT140 in early bone healing of tooth extraction sockets // Oral Dis. – 2022. – Vol. 28 (4). – P. 1188-1197.
3. De Sousa Gomes P., Daugela P., Poskevicius L., Mariano L., Fernandes M.H. Molecular and Cellular Aspects of Socket Healing in the Absence and Presence of Graft Materials and Autologous Platelet Concentrates: A Focused Review // J Oral Maxillofac Res. – 2019. – Vol. 10(3). – P. e2.
4. Dolgalev Al.Al., Svyatoslavov D.S., Pout V.A., Reshetov I.V., Kastyro I.V. Effectiveness of the Sequential Use of Plastic and Titanium Implants for Experimental Replacement of the Mandibular Defect in Animals using Preliminary Digital Design // Doklady Biochemistry and Biophysics. – 2021. – Vol. 496. – P. 36-39.
5. Dragunova S.G., Reshetov I.V., Kosyreva T.F., Severin A.E., Khamidulin G.V., Shmaevsky P.E., A Inozemtsev.N., Popadyuk V.I., Kastyro I.V., Yudin D.K., Yunusov T.Yu., Kleyman V.K., Bagdasaryan V.V., Alieva S.I., Chudov R.V., Kuznetsov N.D., Pinigina I.V., Skopich A.A., Kostyaeva M.G. Comparison of the Effects of Septoplasty and Sinus Lifting Simulation in Rats on Changes in Heart Rate Variability // Doklady Biochemistry and Biophysics. – 2021. – Vol. 498. – P. 165-169.
6. Miroshnychenko A., Ibrahim S., Azab M., Roldan Y., Martinez J.P.D., Tamilselvan D., He L., Little J.W., Urquhart O., Tampi M., Polk D.E., Moore P.A., Hersh E.V., Claytor B., Carrasco-Labra A., Brignardello-Petersen R. Acute Postoperative Pain Due to Dental Extraction in the Adult Population: A Systematic Review and Network Meta-analysis // J Dent Res. – 2023. – Vol. 102 (4). – P. 391-401.
7. Dragunova S., Samoilova M., Ganshin I., Chernolev A. Heart Rate Variability, Pain Syndrome and Cortisol Concentration in Oral Fluid During Sinus-Lifting And Dental Implantation Otorhinolaryngology // Head and Neck Pathology (ORLHNP). – 2023. – Vol. 2 (4). – P. 31-36.
8. Takahashi S., Kikuchi R., Ambe K., Nakagawa T., Takada S., Ohno T., et al. Lymphangiogenesis and Nos Localization in Healing Process after Tooth Extraction in Akita Mouse // Bull Tokyo Dent Coll. – 2016. – Vol. 57(3). – P. 121-31.
9. Devlin H., Sloan P. Early Bone Healing Events in the Human Extraction Socket // Int J Oral Maxillofac Surg. – 2002. – Vol. 31(6). – P. 641-5.

10. Dragunova S.G., Kosyreva T.F., Khamidulin G.V., Shmaevsky P.E., Ermakova N.V., Severin A.E., Torshin V.I., Kastyro I.V., Scopich A.A., Gordeev D.V., Sedelnikova A.D., Kuznetsov N.D., Popadyuk V.I., Yudin D.K. Assessment of the impact of closed sinus lifting on changes in the autonomic nervous system in the early postoperative period. Head and neck. *Russian Journal*, 2022, Vol. 10(1), pp. 8-15.
11. Yudin D.K., Mozgovoy V.V., Kosyreva T.F., Popadyuk V.I., Kastyro I.V., Dragunova S.G. Prevention of anesthesiological complications during dental implantation. Head and neck. Russian Journal Head and neck. *Russian Journal*, 2022, Vol. 10(3), pp. 60-63.
12. Lin G.H., Suárez López Del Amo F., Wang H.L. Laser therapy for treatment of peri-implant mucositis and peri-implantitis: An American Academy of Periodontology. *J. Periodontol*, 2018, Vol. 89 (7), pp. 766-782.
13. Shimorsky M.I., Korchazhkina N.B., Panin A.M., Tsitsiashvili A.M. Features of the use of laser therapy in the rehabilitation of patients after surgical dental interventions. *Physiotherapist*, 2023, Vol. 6, pp. 93-101.
14. Shilin S.S., Spirin E.A, Antonyana A.A., Dolgonovskaya A.S., Piskarev D.V., Popadyuk VI., Kastyro I.V., Ganshin I.B., Vasyakova S.M. The Role of IL-10 G-1082A Polymorphism in Hypertrophy of the Pharyngeal Tonsil. *Molecular Genetics, Microbiology and Virology*, 2023, Vol. 38 (3), pp. 177-184.
15. Younis W.H., Al-Rawi N.H., Mohamed M.A., Yaseen N.Y. Molecular Events on Tooth Socket Healing in Diabetic Rabbits. *Br J Oral Maxillofac Surg*, 2013, Vol. 51 (8), pp. 932-936.
16. Pergolizzi J.V., Magnusson P., LeQuang J.A., Gharibo C., Varrassi G. The pharmacological management of dental pain. *Expert Opin Pharmacother*, 2020, Vol. 21 (5), pp. 591-601.
17. Lodi G., Azzi L., Varoni E.M., Pentenero M., Del Fabbro M., Carrassi A., Sardella A, Manfredi M. Antibiotics to prevent complications following tooth extractions. *Cochrane Database Syst Rev*, 2021, Vol. 2 (2), pp. CD003811
18. Ghosh A., Aggarwal V.R., Moore R. Aetiology, Prevention and Management of Alveolar Osteitis-A Scoping Review. *J Oral Rehabil*, 2022, Vol. 49 (1), pp. 103-113.
19. Razina I.N., Lomiashvili L.M., Nedoseko V.B. Non-surgical treatments of complications after dental implantation. Perspectives for infrared laser light in the treatment of mucositis and peri-implantitis. *Laser Medicine*, 2020, Vol. 24 (1), pp. 49-56.
20. Berni M., Brancato A.M., Torriani C., Bina V., Annunziata S., Cornella E., Trucchi M., Jannelli E., Mosconi M., Gastaldi G., Caliogna L., Grassi F.A., Pasta G. The Role of Low-Level Laser Therapy in Bone Healing: Systematic Review. *Int J Mol Sci*, 2023, Vol. 24 (8), pp. 7094.
21. Menchisheva Y., Menzhanova D., Espolayeva A., Azhibekov A., Mirzakulova U., Sagatbayev A., Uglanov Z., Toregeldi G., Tsvetanov Tsokov K. Combined use of PRPP, diode laser and piezosurgery device improves reparative osteogenesis previously to dental implants placement. *Asian J Surg*, 2024, Vol. S1015-9584(24), pp. 02130-02134.
22. Khadra M. The effect of low level laser irradiation on implant-tissue interaction. In vivo and in vitro studies. *Swed. Dent. J. Suppl*, 2005, Vol. 172, pp. 1-63.
23. Theodoro L.H., Marcantonio R.A.C., Wainwright M., Garcia V.G. LASER in periodontal treatment: is it an effective treatment or science fiction? *Braz Oral Res*, 2021, Vol. 35 (Supp 2), pp. e099.
24. Khadra M., Lyngstadaas S.P., Haanaes H.R. et al. Effect of laser therapy on attachment, proliferation and differentiation of human osteoblast-like cells cultured on titanium implant material. *Biomaterials*, 2005, Vol. 26 (17), pp. 3503-350.
25. Memarian J., Ketabi M., Amini S. The effect of low-level laser 810 nm and light-emitting diodephotobiomodulation (626 nm) on the stability of the implant and inflammatory markers interleukin-1 beta and prostaglandin E2, around implants. *Dent. Res. J. (Isfahan)*, 2018, Vol. 15 (4), pp. 283-288.
26. Chellini F., Giannelli M., Tani A. et al. Mesenchymal stromal cell and osteoblast responses to oxidized titanium surfaces pre-treated with λ = 808 nm GaAlAs diode laser or chlorhexidine: in vitro study. *Lasers Med Sci*, 2017, Vol. 32 (6), pp. 1309-1320.
27. Marom R., Rabenhorst B.M., Morello R. Osteogenesis imperfecta: an update on clinical features and therapies. *Eur J Endocrinol*, 2020, Vol. 183 (4), pp. R95-R106.

10. Dragunova S.G., Kosyreva T.F., Khamidulin G.V., Shmaevsky P.E., Ermakova N.V., Severin A.E., Torshin V.I., Kastyro I.V., Scopich A.A., Gordeev D.V., Sedelnikova A.D., Kuznetsov N.D., Popadyuk V.I., Yudin D.K. Assessment of the impact of closed sinus lifting on changes in the autonomic nervous system in the early postoperative period. Head and neck // Russian Journal. – 2022. – Vol. 10(1). – P. 8-15.
11. Yudin D.K., Mozgovoy V.V., Kosyreva T.F., Popadyuk V.I., Kastyro I.V., Dragunova S.G. Prevention of anesthesiological complications during dental implantation. Head and neck. Russian Journal Head and neck // Russian Journal. – 2022. – Vol. 10(3). – P. 60-63.
12. Lin G.H., Suárez López Del Amo F., Wang H.L. Laser therapy for treatment of peri-implant mucositis and peri-implantitis: An American Academy of Periodontology // J. Periodontol. – 2018. – Vol. 89 (7). – P. 766-782.
13. Shimorsky M.I., Korchazhkina N.B., Panin A.M., Tsitsiashvili A.M. Features of the use of laser therapy in the rehabilitation of patients after surgical dental interventions // Physiotherapist. – 2023. – Vol. 6. – P. 93-101.
14. Shilin S.S., Spirin E.A, Antonyana A.A., Dolgonovskaya A.S., Piskarev D.V., Popadyuk VI., Kastyro I.V., Ganshin I.B., Vasyakova S.M. The Role of IL-10 G-1082A Polymorphism in Hypertrophy of the Pharyngeal Tonsil // Molecular Genetics, Microbiology and Virology. – 2023. – Vol. 38 (3). – P. 177-184.
15. Younis W.H., Al-Rawi N.H., Mohamed M.A., Yaseen N.Y. Molecular Events on Tooth Socket Healing in Diabetic Rabbits // Br J Oral Maxillofac Surg. – 2013. – Vol. 51 (8). – P. 932-6.
16. Pergolizzi J.V., Magnusson P., LeQuang J.A., Gharibo C., Varrassi G. The pharmacological management of dental pain // Expert Opin Pharmacother. – 2020. – Vol. 21 (5). – P. 591-601.
17. Lodi G., Azzi L., Varoni E.M., Pentenero M., Del Fabbro M., Carrassi A., Sardella A, Manfredi M. Antibiotics to prevent complications following tooth extractions // Cochrane Database Syst Rev. – 2021. – Vol. 2 (2). – P. CD003811
18. Ghosh A., Aggarwal V.R., Moore R. Aetiology, Prevention and Management of Alveolar Osteitis-A Scoping Review // J Oral Rehabil. – 2022. – Vol. 49 (1). – P. 103-113.
19. Razina I.N., Lomiashvili L.M., Nedoseko V.B. Non-surgical treatments of complications after dental implantation. Perspectives for infrared laser light in the treatment of mucositis and peri-implantitis // Laser Medicine. – 2020. – Vol. 24 (1). – P. 49-56.
20. Berni M., Brancato A.M., Torriani C., Bina V., Annunziata S., Cornella E., Trucchi M., Jannelli E., Mosconi M., Gastaldi G., Caliogna L., Grassi F.A., Pasta G. The Role of Low-Level Laser Therapy in Bone Healing: Systematic Review // Int J Mol Sci. – 2023. – Vol. 24 (8) . – P. 7094.
21. Menchisheva Y., Menzhanova D., Espolayeva A., Azhibekov A., Mirzakulova U., Sagatbayev A., Uglanov Z., Toregeldi G., Tsvetanov Tsokov K. Combined use of PRPP, diode laser and piezosurgery device improves reparative osteogenesis previously to dental implants placement // Asian J Surg. – 2024. – Vol. S1015-9584(24). – P. 02130-02134.
22. Khadra M. The effect of low level laser irradiation on implant-tissue interaction. In vivo and in vitro studies // Swed. Dent. J. Suppl. – 2005. – Vol. 172. – P. 1-63.
23. Theodoro L.H., Marcantonio R.A.C., Wainwright M., Garcia V.G. LASER in periodontal treatment: is it an effective treatment or science fiction? // Braz Oral Res. – 2021. – Vol. 35 (Supp 2). – P. e099.
24. Khadra M., Lyngstadaas S.P., Haanaes H.R. et al. Effect of laser therapy on attachment, proliferation and differentiation of human osteoblast-like cells cultured on titanium implant material // Biomaterials. – 2005. – Vol. 26 (17). – P. 3503-350.
25. Memarian J., Ketabi M., Amini S. The effect of low-level laser 810 nm and light-emitting diodephotobiomodulation (626 nm) on the stability of the implant and inflammatory markers interleukin-1 beta and prostaglandin E2, around implants // Dent. Res. J. (Isfahan). – 2018. – Vol. 15 (4). – P. 283-288.
26. Chellini F., Giannelli M., Tani A. et al. Mesenchymal stromal cell and osteoblast responses to oxidized titanium surfaces pre-treated with λ = 808 nm GaAlAs diode laser or chlorhexidine: in vitro study // Lasers Med Sci. – 2017; 32 (6). – P. 1309-1320.
27. Marom R., Rabenhorst B.M., Morello R. Osteogenesis imperfecta: an update on clinical features and therapies // Eur J Endocrinol. 2020. – Vol. 183 (4). – P. R95-R106.

28. Carroll R.S., Donenfeld P., McGreal C., Franzone J.M., Kruse R.W., Preedy C., Costa J., Dirnberger D.R., Bober M.B. Comprehensive pain management strategy for infants with moderate to severe osteogenesis imperfecta in the perinatal period. *Paediatr Neonatal Pain*, 2021, Vol. 3 (4), pp. 156-16.
29. Dlesk T.E., Larimer K. Multimodal Pain Management of Children Diagnosed with Osteogenesis Imperfecta: An Integrative Literature Review. *Pain Manag Nurs*, 2023, Vol. 24 (1), pp. 102-110.
30. Rodriguez Celin M., Kruger K.M., Caudill A., Murali C.N., Nagamani S.C.S. Members of the Brittle Bone Disorders Consortium (BBDC); Smith P.A., Harris G.F. A multicenter study to evaluate pain characteristics in osteogenesis imperfecta. *Am J Med Genet A*, 2023, Vol. 191 (1), pp. 160-172.
31. Shepherd W.S., Wiese A.D., Cho H.E., Rork W.C., Baig M.U., Kostick K.M., Nguyen D., Carter E.M. Members of the BBDC; Murali C.N., Robinson M.E., Schneider S.C., Lee B., Sutton V.R., Storch E.A. Psychosocial Outcomes of Pain and Pain Management in Adults with Osteogenesis Imperfecta: A Qualitative Study. *J Clin Psychol Med Settings*, 2024, Vol. 31 (3), pp. 614-627.
32. Gonçalves F.C., Mascaro B.A., Oliveira G.J.P.L., Spolidório L.C., Marcantonio R.A.C. Effects of red and infrared laser on post extraction socket repair in rats subjected to alendronate therapy. *Braz Oral Res*, 2023, Vol. 37, pp. e048.
33. Kastyro I.V., Romanko Yu.S., Muradov G.M., Popadyuk V.I., Kalmykov I.K., Kostyaeva M.G., Gushchina Yu.Sh., Dragunova S.G. Photobiomodulation of acute pain syndrome after septoplasty. Biomedical Photonics, 2021. – Vol. 10 (2). – P. 34-41.
34. Muradov G.M., Popadyuk V.I., Kastyro I.V., Chernolev A.I., Mikhalskaia P.V. Photobiomodulating Therapy in Early Rehabilitation of Patients after Septoplasty. *ORLHNP. ISCPP2023 ABSTRACT BOOK*, 2023, Vol. 2(3), pp. 20.
35. Kastyro I.V., Popadyuk V.I., Muradov G.M., Reshetov I.V. Low-Intensity Laser Therapy As a Method to Reduce Stress Responses after Septoplasty. *Dokl Biochem Biophys*, 2021, Vol. 500 (1), pp. 300-303.
36. Dragunova S.G., Gordeev D.V., Chernolev A.I., Shishkova D.A., Shalamov K.P., Popadyuk V.I., Kastyro I.V., Senin N.E., Kartasheva A.F., I.B. Ganshin, Barannik M.I., Sarygin P.V. Role of surgical trauma in the hippocampal dopaminergic system response in simulated surgical interventions on the nasal cavity, paranasal sinuses, and alveolar process of the maxilla in rats. Head and neck. *Russian Journal*, 2024, Vol. 12(3), pp. 16-27.
37. Kotov V.N., Kastyro I.V., Ganshin I.B., Popadyuk V.I., Dragunova S.G., Khodorovich O.S., Kartasheva A.F., Barannik M.I., Sarygin P.V. The Role of Photobiomodulation Therapy in Reducing Stress-Induced Changes in the Hippocampus of Rats during Septoplasty Modeling. *Doklady Biochemistry and Biophysics*, 2025, Vol. 520, pp. Iss.1. in print DOI: 10.1134/S1607672924601033
38. Romanko Yu.S., Reshetov I.V. Experimental and clinical combined photodynamic therapy for malignant and premalignant lesions using various types of radiation. *Siberian Journal of Oncology*, 2024, Vol. 23(4), pp. 141-151.
39. Reshetov I.V., Korenev S.V., Romanko Yu.S. Forms of cell death and targets at photodynamic therapy. *Siberian Journal of Oncology*, 2022, Vol. 21(5), pp. 149-154.
40. Reshetov I.V., Romanko Yu.S. Pharmaceutical and experimental-clinical aspects of combined photodynamic therapy of malignant tumors and precancerous tumors using chemotherapy. *Siberian Journal of Oncology. Siberian Journal of Oncology*, 2022, Vol. 21(5).

28. Carroll R.S., Donenfeld P., McGreal C., Franzone J.M., Kruse R.W., Preedy C., Costa J., Dirnberger D.R., Bober M.B. Comprehensive pain management strategy for infants with moderate to severe osteogenesis imperfecta in the perinatal period // Paediatr Neonatal Pain. – 2021. – Vol. 3 (4). – P. 156-16.
29. Dlesk T.E., Larimer K. Multimodal Pain Management of Children Diagnosed with Osteogenesis Imperfecta: An Integrative Literature Review // Pain Manag Nurs. – 2023. – Vol. 24 (1). – P. 102-110.
30. Rodriguez Celin M., Kruger K.M., Caudill A., Murali C.N., Nagamani S.C.S. Members of the Brittle Bone Disorders Consortium (BBDC); Smith P.A., Harris G.F. A multicenter study to evaluate pain characteristics in osteogenesis imperfecta // Am J Med Genet A. – 2023. – Vol. 191 (1). – P. 160-172.
31. Shepherd W.S., Wiese A.D., Cho H.E., Rork W.C., Baig M.U., Kostick K.M., Nguyen D., Carter E.M. Members of the BBDC; Murali C.N., Robinson M.E., Schneider S.C., Lee B., Sutton V.R., Storch E.A. Psychosocial Outcomes of Pain and Pain Management in Adults with Osteogenesis Imperfecta: A Qualitative Study // J Clin Psychol Med Settings. – 2024. – Vol. 31 (3). – P. 614-627.
32. Gonçalves F.C., Mascaro B.A., Oliveira G.J.P.L., Spolidório L.C., Marcantonio R.A.C. Effects of red and infrared laser on post extraction socket repair in rats subjected to alendronate therapy // Braz Oral Res. – 2023. – Vol. 37. – P. e048.
33. Kastyro I.V., Romanko Yu.S., Muradov G.M., Popadyuk V.I., Kalmykov I.K., Kostyaeva M.G., Gushchina Yu.Sh., Dragunova S.G. Photobiomodulation of acute pain syndrome after septoplasty // Biomedical Photonics. – 2021. – Vol. 10 (2). – P. 34-41.
34. Muradov G.M., Popadyuk V.I., Kastyro I.V., Chernolev A.I., Mikhalskaia P.V. Photobiomodulating Therapy in Early Rehabilitation of Patients after Septoplasty // ORLHNP. ISCPP2023 ABSTRACT BOOK. – 2023. – Vol. 2(3). – P. 20.
35. Kastyro .IV., Popadyuk V.I., Muradov G.M., Reshetov I.V. Low-Intensity Laser Therapy As a Method to Reduce Stress Responses after Septoplasty // Dokl Biochem Biophys. – 2021. – Vol. 500 (1). – P. 300-303.
36. Dragunova S.G., Gordeev D.V., Chernolev A.I., Shishkova D.A., Shalamov K.P., Popadyuk V.I., Kastyro I.V., Senin N.E., Kartasheva A.F., I.B. Ganshin, Barannik M.I., Sarygin P.V. Role of surgical trauma in the hippocampal dopaminergic system response in simulated surgical interventions on the nasal cavity, paranasal sinuses, and alveolar process of the maxilla in rats. Head and neck // Russian Journal. – 2024. – Vol. 12(3). – P. 16-27.
37. Kotov V.N., Kastyro I.V., Ganshin I.B., Popadyuk V.I., Dragunova S.G., Khodorovich O.S., Kartasheva A.F., Barannik M.I., Sarygin P.V. The Role of Photobiomodulation Therapy in Reducing Stress-Induced Changes in the Hippocampus of Rats during Septoplasty Modeling // Doklady Biochemistry and Biophysics. – 2025. – Vol. 520. – P. Iss.1. *in print* DOI: 10.1134/S1607672924601033
38. Romanko Yu.S., Reshetov I.V. Experimental and clinical combined photodynamic therapy for malignant and premalignant lesions using various types of radiation // Siberian Journal of Oncology. – 2024. – Vol. 23(4). – P. 141-151.
39. Reshetov I.V., Korenev S.V., Romanko Yu.S. Forms of cell death and targets at photodynamic therapy // Siberian Journal of Oncology. – 2022. – Vol. 21(5). – P. 149-154.
40. Reshetov I.V., Romanko Yu.S. Pharmaceutical and experimental-clinical aspects of combined photodynamic therapy of malignant tumors and precancerous tumors using chemotherapy // Siberian Journal of Oncology. Siberian Journal of Oncology. – 2022. – Vol. 21(5).

INVESTIGATION OF METHODS FOR MODELING LIGHT PROPAGATION IN MULTILAYER BIOLOGICAL TISSUES FOR CALCULATING THE ABSORBED DOSE OF LASER RADIATION

Krivetskaya A.A.[1,2], Savelieva T.A.[1,2], Kustov D.M.[1], Levkin V.V.[3], Kharnas S.S.[3], Loschenov V.B.[1,2]
[1]Prokhorov General Physics Institute of the Russian Academy of Sciences, Moscow, Russia
[2]Institute of Engineering Physics for Biomedicine, National Research Nuclear University MEPhI, Moscow, Russia
[3]Department of Faculty Surgery No. 1, I.M. Sechenov First Moscow State Medical University, Moscow, Russia

Abstract

Studying the interaction of optical wavelength radiation with biological tissues can be used in various biomedical applications, including estimating the absorbed dose of laser radiation during laser-induced therapy. The fraction of absorbed radiation can be estimated using Monte Carlo and adding-doubling simulations. In this paper, we compare the simulation results obtained using the two methods for multilayered models of biological tissues of the trachea and colon. Both methods are used to calculate the absorbed dose based on the specified optical properties of tissues under several types of illumination. Similar incident beam geometries demonstrated repeatability of 94±3% for a collimated beam and 95±3% for an isotropic/diffuse source. The advantage of the adding-doubling method is its higher computational speed compared to the Monte Carlo method, while Monte Carlo simulation allows for varying a larger number of parameters when specifying the illumination conditions of the sample. The data obtained can be used to optimize dosimetry in photodynamic therapy.

Key words: optical property, adding-doubling method, Monte Carlo method, multilayer biological tissue, absorbed dose, laser dosimetry.

Contacts: Krivetskaya A.A., e-mail: annakrivetskaya1998@gmail.com

For citations: Krivetskaya A.A., Savelieva T.A., Kustov D.M., Levkin V.V., Kharnas S.S., Loschenov V.B. Investigation of methods for modeling light propagation in multilayer biological tissues for calculating the absorbed dose of laser radiation, *Biomedical Photonics*, 2026, vol. 15, no. 1, pp. 19–29. doi: 10.24931/2413–9432–2026–15-1-19-29

ИССЛЕДОВАНИЕ МЕТОДОВ МОДЕЛИРОВАНИЯ РАСПРОСТРАНЕНИЯ СВЕТА В МНОГОСЛОЙНЫХ БИОЛОГИЧЕСКИХ ТКАНЯХ ДЛЯ РАСЧЕТА ПОГЛОЩЕННОЙ ДОЗЫ ЛАЗЕРНОГО ИЗЛУЧЕНИЯ

А.А. Кривецкая[1,2], Т.А. Савельева[1,2], Д.М. Кустов[1], В.В. Левкин[3], С.С. Харнас[3], В.Б. Лощенов[1,2]
[1]Институт общей физики им. А.М. Прохорова Российской академии наук, Москва, Россия
[2]Национальный исследовательский ядерный университет «МИФИ», Москва, Россия
[3]Университетская Клиническая больница №1 Первого МГМУ им. Сеченова, Москва, Россия

Резюме

Изучение процессов взаимодействия излучения в оптическом диапазоне длин волн с биологическими тканями может применяться для различных биомедицинских применений, в том числе для оценки поглощенной дозы лазерного излучения при проведении лазерно-индуцированной терапии. Оценка доли поглощенного излучения может осуществляться при помощи моделирования методами Монте-Карло и удвоения-добавления. В данной работе проведен сравнительный анализ результатов моделирования двумя методами для многослойных моделей биологических тканей трахеи и толстой кишки. Оба метода применены для расчета поглощенной дозы по заданным оптическим свойствам тканей при нескольких видах освещения. Схожие геометрии пучка падающего излучения показали повторяемость с точностью 94±3% для коллимированного пучка и 95±3% для изотропного/диффузного источника. Преимуществом метода удвоения-добавления является большая вычислительная скорость по сравнению с методом Монте-Карло, в то

время как при моделировании методом Монте-Карло можно варьировать большее количество параметров при задании условий освещения образца. Полученные данные могут использоваться для оптимизации дозиметрии в фотодинамической терапии.

Ключевые слова: оптическое свойство, метод удвоения-добавления, метод Монте-Карло, многослойная биологическая ткань, поглощенная доза, лазерная дозиметрия.

Контакты: Кривецкая А.А., e-mail: annakrivetskaya1998@gmail.com

Для цитирования: Кривецкая А.А., Савельева Т.А., Кустов Д.М., Левкин В.В., Харнас С.С., Лощенов В.Б. Исследование методов моделирования распространения света в многослойных биологических тканях для расчета поглощенной дозы лазерного излучения // Biomedical Photonics. – 2026. –Т. 15, № 1. – С. 19–29. doi: 10.24931/2413–9432–2026–15-1-19-29

Introduction

In biomedical optics, the results of researches on modeling the propagation of light in biological tissues can be used for various biomedical applications, such as spectral diagnostics of photodynamic therapy, optical biopsy and monitoring of tissue oxygenation (StO_2), as well as for predicting the absorbed dose of laser radiation during laser-induced therapy [1, 2]. For a more accurate description of the interaction processes of optical radiation with real tissues, it is necessary to take into account their multilayeredness, since the optical properties of different layers can vary significantly, which reduces accuracy if the tissue is considered homogeneous.

Light propagation in tissue is determined by the optical properties of the medium: the absorption coefficient (μ_a), the scattering coefficient (μ_s), and the anisotropy factor (g). The absorption coefficient determines the probability of photon absorption per unit path length in the tissue. The main absorbers in biological tissues are hemoglobin, water, lipids, and melanin [3]. The scattering coefficient describes how often a photon changes direction in a medium. In the ultraviolet and far-infrared ranges, the contribution of scattering is relatively smaller compared to intense absorption. In the spectral range of 650-1000 nm, scattering dominates over absorption, creating the biological transparency window – the range in which optical radiation penetrates most deeply into biological tissue [4, 5]. The anisotropy factor (the average cosine of the scattering angle) determines the direction of light scattering.

Light propagation in biological tissues, which are turbid, i.e., highly scattering, media, can be described using radiative transfer theory. This theory ignores certain wave properties of light, such as interference and polarization, and considers only the transfer of light energy in the medium. It is assumed that the particle energy remains unchanged on average during interaction, and the analysis is limited to studying the propagation of monochromatic photons. The fundamental equation of radiative transfer theory incorporates the optical properties of the medium (μ_a and μs). Spectral measurements of multilayered biological tissues can yield values for parameters such as diffuse reflectance (R_d) and transmittance (T_d), whose values are determined by the optical properties of the object being studied and the measurement conditions.

Various approximations are used to solve the equations of radiative transfer theory. One of the standard methods for numerical solution is the Monte Carlo (MC) method [6, 7], which provides high accuracy due to stochastic modeling of photon trajectories, allows for the presence of layers with different values of optical properties to be taken into account, but requires significant computing resources and, accordingly, time costs [8]. An exact solution to the radiative transfer equation in biological tissues is only possible numerically, making the Monte Carlo method one of the most widely available and accurate tools for modeling diffuse reflectance and transmittance. The Monte Carlo method can be used both to solve the direct problem – modeling the diffuse reflectance and transmittance of a three-layer model of biological tissue based on given optical properties – and to solve the inverse problem – reconstructing optical properties based on diffuse reflectance and transmittance values [9]. A series of papers, including the first examples of simulating diffuse reflectance from a semi-infinite scattering medium and subsequent scalable methods for multilayer geometries, showed that the Monte Carlo method can take into account arbitrary distributions of μ_a, μ_s, and g, as well as complex geometries and illumination conditions [10]. In particular, photon trajectory scaling methods can significantly reduce calculation time for a wide range of optical parameters [11].

The adding-doubling (A-D) method can also be used to account for the multilayer nature of biological tissues. It allows for the rapid calculation of integrated reflectance and transmittance coefficients for layered media using the reflectance and transmittance matrices of individual layers. Due to its high speed, the A-D method is widely used to describe the light field in multilayered tissues and validate more complex models. However, the classical A-D method assumes the homogeneity of each layer and does not account for local inclusions. It is also limited in its analysis of the spatiotemporal structure of

the field, which limits its application in problems with strong heterogeneity [12, 13].

Systematic comparative studies of the effects of layers with different μ_a, μ_s, and g on diffuse reflectance and transmittance in multilayer fabrics are scarce. Based on publicly available data, there is only one study comparing Monte Carlo and adding-doubling methods for a single-layer sample [14]. In this paper, the results of modeling diffuse reflection and transmission in models of multilayer biological tissues using Monte Carlo and adding-doubling methods are compared.

Materials and methods

Algorithms describing the propagation of light in multilayer highly scattering media

The Monte Carlo method is one of the most frequently used methods for numerically solving the equation of radiative transfer theory. It involves determining the trajectory of a photon in a medium before it is absorbed or exits the medium based on the probabilities of absorption, scattering, and the scattering angle. These probabilities are determined by the optical properties of the medium – the absorption and scattering coefficients, as well as the anisotropy factor. Monte Carlo simulation of light propagation in tissue was performed for various incident beam geometries: from a point downward, from a point isotropically, from a fiber with a radius of 0.125 mm and an numerical aperture (NA) of 0.37, a collimated beam with a radius of 0.125 mm, and a Gaussian beam with a radius of 0.125 mm. A schematic representation of these incident beam geometries is shown in Fig. 1. In addition to the values of diffuse reflection and transmission, the Monte Carlo method makes it possible to determine the values of the fraction of absorbed radiation, which can be used to estimate the absorbed dose of laser radiation during laser-induced therapy.

The adding-doubling method can also be used to solve the radiative transfer equation. It was proposed by van de Hulst in 1963. The algorithm, as its name suggests, consists of two parts. First, for each set of optical properties corresponding to different layers in the sample, a "doubling" process is performed. In the first step, the diffuse reflectance (R_d) and transmittance (T_d) values are calculated for a thin layer whose thickness allows for only single scattering. The thickness is then doubled, and the R_d and T_d values are determined for the new thickness. This process is repeated until the final thickness of the layer with a given set of optical properties is reached. After the "doubling" process is complete for each set of optical properties, an "addition" process is performed, which involves calculating the diffuse reflectance and transmittance values for the entire sample, including layers with different sets of optical properties. To simulate the diffuse reflection and transmission of a multilayer models of biological tissues based on given optical properties, an algorithm was used, implemented in the Python programming language using the numpy, scipy, and iadpython libraries developed by Scott Prahl [15]. Light propagation in tissue was simulated for two incident beam geometries: collimated and diffuse. The fraction of absorbed radiation (A) was determined as $A = 1 - R_d - T_d$.

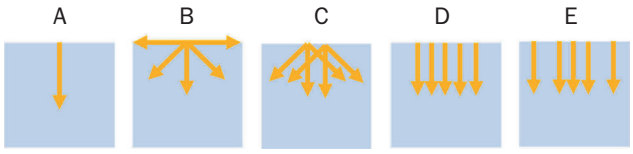

Рис. 1. Варианты геометрии падающего излучения при попадании света в ткань до взаимодействия с рассеивателями и поглотителями: A – из точки вниз; B – из точки изотропно; C – из волокна с заданным радиусом и апертурой; D – коллимированный пучок заданного радиуса; E – гауссов пучок заданного радиуса.
Fig. 1. Geometry options for incident radiation when light enters the tissue before interacting with diffusers and absorbers: A – from a point downwards; B – from a point isotropically; C – from a fiber with a given radius and aperture; D – collimated beam of a given radius; E – Gaussian beam of a given radius.

Mathematical models of multilayer media

In this study, the walls of hollow organs, such as the trachea and colon, were chosen as examples of multilayered tissues to allow considering different illumination conditions. Absorbed dose dosimetry is a practically significant task, for example, for the personalization of the photodynamic therapy (PDT) of the organs of the gastrointestinal tract, which performs for the treatment of gastrointestinal cancers as an adjunct to surgery, as well as for small tumors and as a palliative treatment [17-19]. As for trachea, secondary neoplasms of this organ are more common than primary tracheal tumors and typically arise from direct invasion of the trachea from primary malignancies in adjacent structures, such as the thyroid gland, lungs, esophagus, head and neck, or larynx. Examples of the effective use of PDT exist for such cases [20, 21], as well as for primary tumors of the trachea [22].

To achieve the objectives of this study, several models of highly scattering media were proposed. First, to compare and verify the modeling results, a single-layer model with optical properties on average relevant to the biological tissues proposed for study (trachea and intestine) was proposed. More complex models were constructed taking into account increasingly accurate representations of the layers in the walls of these hollow organs. Their geometries, optical properties and thickness (d) are presented in Tables 1-5.

To perform the simulation, the tracheal wall was represented as a four or six layer structure with specified optical properties and thicknesses. The parameters for each layer, for which the simulation was performed, such

Таблица 1
Оптические свойства однослойной модели биологических тканей

Table 1
Optical properties of a single-layer model of biological tissues

Параметр Parameter	Значения Values
μ_a, cm^{-1}	3
μ_s, cm^{-1}	130
g	0.77
n	1.38
d, mm	2

Таблица 2
Оптические свойства слоев модели биологической ткани, имитирующей слой надхрящницы трахеи между слизистыми на длине волны 542 нм

Table 2
Optical properties of the layers of the biological tissue model simulating the perichondrium layer of the trachea between the mucosal membranes at a wavelength of 542 nm

Параметр Parameter	Слои 1, 3 (слизистая) Layers 1, 3 (mucosa)	Слой 2 (надхрящница) Layer 2 (perichondrium)
μ_a, cm^{-1}	3.6	6.81
μ_s, cm^{-1}	142	120
g	0.73	0.79
n	1.38	1.38
d, mm	0.45	0.1

Таблица 3
Оптические свойства четырехслойной модели трахеи

Table 3
Optical properties of the four-layer trachea model

Слои Layers	Толщина слоя, мм Layer thickness, mm	μ_a, cm^{-1}, μ_s, cm^{-1}, g	542 nm	630 nm
слизистая mucosa	0.35	μ_a	3.6	2
		μ_s	142	139
		g	0.73	0.78
подслизистая submucosa	0.55	μ_a	2.8	1.6
		μ_s	140	138
		g	0.72	0.77
фиброзно - хрящевая оболочка fibrocartilaginous membrane	1	μ_a	4	1.1
		μ_s	120	117
		g	0.79	0.81
адвентиция adventitia	0.1	μ_a	3.5	1.4
		μ_s	78	70
		g	0.86	0.89

as thickness, scattering and absorption coefficients, and the anisotropy factor, are presented in Tables 3 and 4 [23–28]. The refractive index for all layers was taken equal to 1.37 [29, 30].

The normal colonic wall thickness ranges from 0 to 2 mm in colonic segments ≥4–6 cm in diameter, from 0.2 to 2.5 mm in colonic segments 3–4 cm in diameter, from 0.3 to 4 mm in colonic segments 2–3 cm in diameter, and from 0.5 to 5 mm in colonic segments 1–2 cm in diameter. The maximum colonic wall thickness reaches 6 and 8 mm in the proximal and distal colon, respectively, if the measured colonic segment demonstrated a lumen width <1 cm [31].

In work [32], measurements were made on 13 human colon samples (adenomal and normal sample in each case) for four tissue types (mucosa/submucosa and muscularis/chorion) using two integrating spheres and laser sources at wavelengths from 476.5 to 532 nm. Optical properties were assessed using the adding-doubling method. For normal tissues at a wavelength of

Таблица 4
Оптические свойства шестислойной модели трахеи

Table 4
Optical properties of the six-layer trachea model

Слои Layers	Толщина слоя, мм Layer thickness, mm	μ_a, cm^{-1}, µs, cm^{-1}, g	542 nm	630 nm
слизистая mucosa	0.35	μ_a	3.6	2
		μ_s	142	139
		g	0.73	0.78
подслизистая submucosa	0.55	μ_a	2.8	1.6
		μ_s	140	138
		g	0.72	0.77
фиброзно - хрящевая оболочка fibrocartilaginous membrane 1 mm	надхрящница perichondrium 0.1	μ_a oxyg.	6.81	1.12
		μ_a deox.	6.54	1.36
		μ_s	120	117
		g	0.79	0.81
	0.8	μ_a	4	1.1
		μ_s	120	117
		g	0.79	0.81
	надхрящница perichondrium 0.1	μ_a oxyg.	6.81	1.12
		μ_a deox.	6.54	1.36
		μ_s	120	117
		g	0.79	0.81
адвентиция adventitia	0.1	μ_a	3.5	1.4
		μ_s	78	70
		g	0.86	0.89

532 nm, the optical properties of the layer containing the mucous and submucosa were represented by the values μ_a = 3.33±0.14 cm^{-1}, μ_s = 208±5.16 cm^{-1}, g = 0.908±0.029, and for the tissues of the muscular layer μ_a = 1.53±0.06 cm^{-1}, μ_s =193±5.05 cm^{-1}, g = 0.941±0.048.

In the work of the same group [33], the optical properties of normal and adenomatous human colon tissues were investigated in vitro at wavelengths of 630, 680, 720, 780, 850 and 890 nm using a titanium-sapphire laser and the inverse Monte Carlo method. For the normal mucosa/submucosa at a wavelength of 630 nm, the values of μ_a = 0.143±0.004 cm^{-1} and μ_s = 208±5.27 cm^{-1} were determined. For the normal muscular layer, μ_a = 0.0997±0.0025 cm^{-1} and μ_s = 203±5.08 cm^{-1}. For the muscular layer/chorion of the human colon, the scattering anisotropy coefficient g at 633 nm was not reported directly in the main study using the integrating sphere. Since the value of the considered parameter increases smoothly with wavelength, and such studies often use a helium-neon laser with a wavelength of 632.8–633 nm, other studies of colon tissue at 633 nm typically use anisotropy coefficients in the range g≈0.94–0.96 for muscular or highly scattering layers of the colon. Thus, a practical estimate for the muscular layer of the colon at 633 nm is g≈0.945±0.01 for normal tissue and slightly higher for adenomatous tissue, suggesting the same monotonic trend extrapolated from the range 532→633 nm.

In the article [34], 20 samples of human colon tissue (10 samples of mucosa and 10 samples of submucosa) were placed in a 0.9% aqueous NaCl solution after resection and stored in it for 8–12 h at a temperature of ~4°C before spectral measurements were carried out. Optical properties were determined using a spectrophotometer with an integrating sphere in the range of 350–2500 nm. To restore the optical properties, the inverse doubling-addition method was used to estimate the initial values, and the inverse Monte Carlo method was used for the final determination. As a result, approximations were obtained for the spectrum of the scattering coefficient of the mucosal membrane by the function $\mu_s(\lambda) = 138.896\lambda^{-3.443} + 14460\lambda^{-0.617}$ and the submucosa by the function $\mu_s(\lambda) = 125.725\lambda^{-3.594} + 999.947\lambda^{-0.368}$, where λ is wavelength in nanometers. This results in values of $\mu_s(\lambda)$ = 300.8 cm^{-1} for the mucosa and $\mu_s(\lambda)$ = 99.3 cm^{-1} for the submucosa at a wavelength of 532 nm, and $\mu_s(\lambda)$ = 270 cm^{-1} for the mucosa and $\mu_s(\lambda)$ = 93 cm^{-1} for the submucosa at a wavelength of 633 nm. This means that the scattering coefficient for the mucosa is approximately three times higher than for the submucosa. Approximations were also obtained for the anisotropy factor of the mucosa and submucosa: $g(\lambda) = 0.77 + 0.18\,[1 - \exp(-(\lambda - 378.7)/111.1)]$ and $g(\lambda) = 0.77 + 0.19\,[1 - \exp(-(\lambda - 380.4)/128.1)]$. The authors also showed that absorption in the mucosa is higher than in the submucosa.

In [35], an inverse adding-doubling method was used to rapidly estimate optical properties based on spectra in the range from 400 to 1000 nm for pre-frozen colon mucosa and early-stage adenocarcinoma samples. For healthy mucosa, the absorption coefficient was 2.5 cm^{-1} at 532 nm and 0.75 cm^{-1} at 633 nm, while the reduced scattering coefficient was 19 cm^{-1} and 15.5 cm^{-1}, respectively. The anisotropy factor at 532 nm was determined to be 0.82, and at 633 nm, 0.865.

The refractive index of the tissues examined was taken from [36] and was 1.38 for mucosa, 1.36 for submucosa and muscle.

Combining the results of the works discussed above, we took for our mathematical model of the intestinal wall the values of optical properties presented in Table 5.

Таблица 5
Оптические параметры трехслойной модели нормальных тканей стенки толстой кишки

Table 5
Optical parameters of a three-layer model of normal colon wall tissues

Слои Layers	Толщина слоя, мм Layer thickness, mm	μ_a, cm^{-1}, μ_s, cm^{-1}, g	542 nm	630 nm
слизистая mucosa	0.4	μ_a	2,78	0,80
		μ_s	204,52	197,60
		g	0,88	0,90
		n	1,38	1,38
подслизистая submucosa	0.4	μ_a	1	0,7
		μ_s	99	93
		g	0,96	0,96
		n	1,36	1,36
мышечный слой muscular layer	2	μ_a	1,53	0,0997
		μ_s	193	203
		g	0,941	0,945
		n	1,36	1,36

Results and discussion

Results of mathematical modeling of light propagation in primary models

Tables 6 and 7 present for comparison the results of doubling-addition and Monte Carlo simulations for simplified models of biological tissues with optical properties in the range corresponding to real values at a wavelength of 542 nm.

The results of the Monte Carlo and adding-doubling algorithms show repeatability under similar illumination conditions (the isotropic source from a point for Monte Carlo can be compared with the diffuse illumination of the doubling-addition method, and the comparison of

conditions under collimated illumination requires no further comment).

Despite the fact that collimated incident beam is not an absolutely adequate model for experimental conditions under illumination through an optical fiber with a given aperture, we see from the Monte Carlo simulation results that these two illumination scenarios are still closer to each other than the isotropic/diffuse radiation source case. In the latter case, we obtain overestimated values for the diffuse reflectance signal.

Results of mathematical modeling of light propagation in trachea models

Tables 8–11 present the results of Monte Carlo and adding-doubling simulations of diffuse reflectance and transmittance values, as well as the fraction of absorbed radiation, for four-layer and six-layer tracheal models at wavelengths of 542 and 630 nm. Figure 2 shows a diagram of the light propagation trajectory in tissues during the recording of a diffuse reflectance and transmittance signal using the example of a four-layer trachea model.

When illuminated from the adventitia, diffuse reflection is expectedly lower due to light scattering, which is almost half as strong in the adventitia as in the mucosa. Moreover, the anisotropy factor is higher in the adventitia, meaning that for the scattering event the scattered photon is more likely to be directed forward, rather than backward, toward the diffuse reflectance signal receiver. This means that the mucosa acts as a kind of highly scattering mirror, reflecting light twice higher than adventitia.

For the six-layer tracheal model, a decrease in the agreement between the Monte Carlo and doubling-addition methods is observed (94±1%) compared to the four-layer model (95±2%). This is due to the fact that the six-layer model contains layers with a high level of

Таблица 6
Полученные путем моделирования распространения света в однослойной модели биологических тканей значения диффузного отражения и пропускания

Table 6
Diffuse reflection and transmission values obtained by simulating light propagation in a single-layer model of biological tissue

	MC	MC	MC	MC	MC	A-D	A-D
	NA 0.37	из точки вниз from a point downwards	изотропный isotropic	коллимированный collimated	Гауссов Gaussian	диффузный diffuse	коллимированный collimated
R_d	0.27	0.27	0.33	0.27	0.27	0.32	0.29
T_d	0.03	0.03	0.02	0.03	0.03	0.03	0.03

Таблица 7
Результаты моделирования для модели, представляющей собой надхрящницу трахеи между слизистыми

Table 7
Simulation results for a model representing the tracheal perichondrium between the mucous membranes

	MC	MC	MC	MC	MC	A-D	A-D
	NA 0.37	из точки вниз from a point downwards	изотропный isotropic	коллимированный collimated	Гауссов Gaussian	диффузный diffuse	коллимированный collimated
R_d	0.269	0.268	0.329	0.267	0.268	0.32	0.29
T_d	0.071	0.072	0.056	0.071	0.071	0.09	0.1

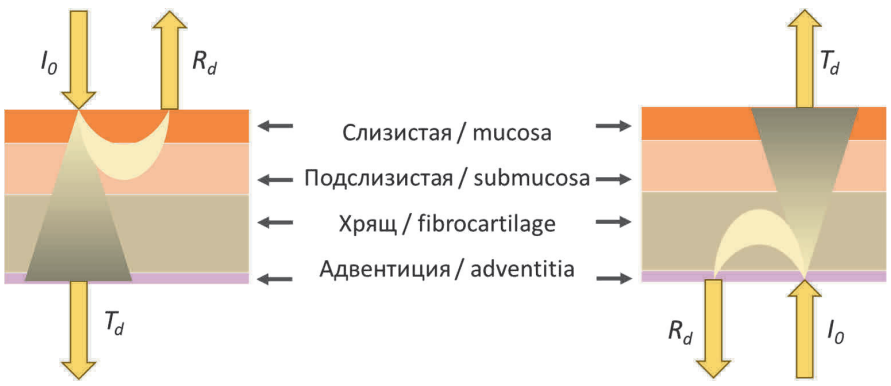

Рис. 2. Схема геометрии освещения (поток падающего излучения I0) и регистрации сигналов диффузного отражения (Rd) и диффузного пропускания (Td).
Fig. 2. Schematic diagram of the illumination geometry (incident radiation flux I0) and registration of diffuse reflection (Rd) and diffuse transmission (Td) signals.

Таблица 8
Результаты моделирования распространения излучения с длиной волны 542 нм в четырехслойной модели трахеи

Table 8
Results of modeling the propagation of radiation at a wavelength of 542 nm in a four-layer model of the trachea

Направление Direction		MC	MC	A-D	MC	A-D
		NA 0.37	диффузный diffuse		коллимированный collimated	
со стороны слизистой from the mucosa	R_d	0.287	0.343	0.351	0.286	0.302
	A	0.700	0.647	0.63	0.702	0.676
	T_d	0.013	0.010	0.019	0.013	0.022
со стороны адвентиции from the adventitia	R_d	0.166	0.216	0.246	0.164	0.212
	A	0.798	0.807	0.737	0.800	0.769
	T_d	0.035	0.027	0.017	0.035	0.019

Таблица 9
Результаты моделирования распространения излучения с длиной волны 630 нм в четырехслойной модели трахеи

Table 9
Results of modeling the propagation of radiation at a wavelength of 630 nm in a four-layer model of the trachea

Направление Direction		MC	MC	A-D	MC	A-D
		NA 0.37	диффузный diffuse		коллимированный collimated	
со стороны слизистой from the mucosa	R_d	0.35	0.40	0.402	0.35	0.369
	A	0.57	0.53	0.513	0.57	0.538
	T_d	0.08	0.06	0.085	0.08	0.093
со стороны адвентиции from the adventitia	R_d	0.30	0.34	0.408	0.29	0.377
	A	0.56	0.54	0.506	0.56	0.528
	T_d	0.14	0.11	0.086	0.14	0.095

Таблица 10
Результаты моделирования распространения излучения с длиной волны 542 нм в шестислойной модели трахеи

Table 10
Results of modeling the propagation of radiation with a wavelength of 542 nm in a six-layer model of the trachea

StO_2	Направление Direction		MC	MC	A-D	MC	A-D
			NA 0.37	диффузный diffuse		коллимированный collimated	
Оксигенированная надхрящница Oxygenated perichondrium	со стороны слизистой from the mucosa	R_d	0.287	0.342	0.340	0.285	0.306
		A	0.705	0.652	0.64	0.707	0.672
		T_d	0.008	0.006	0.020	0.008	0.022
	со стороны адвентиции from the adventitia	R_d	0.146	0.182	0.225	0.145	0.193
		A	0.830	0.801	0.76	0.831	0.79
		T_d	0.024	0.017	0.015	0.024	0.017
Дезоксигенированная надхрящница Deoxygenated perichondrium	со стороны слизистой from the mucosa	R_d	0.286	0.342	0.339	0.285	0.305
		A	0.705	0.651	0.644	0.707	0.675
		T_d	0.008	0.007	0.017	0.008	0.020
	со стороны адвентиции from the adventitia	R_d	0.148	0.184	0.227	0.147	0.195
		A	0.828	0.798	0.758	0.828	0.788
		T_d	0.024	0.018	0.015	0.025	0.017

blood filling (perichondrium), for which the absorption coefficient and the reduced scattering coefficient become closer, and the assumptions of the diffusion approximation of the radiative transfer theory no longer satisfy the conditions of light propagation [37]. Moreover, the modeling results differ to a greater extent when illuminated from the adventitia. This is explained by the fact that in this case the thin, but highly absorbing, perichondrium layer is closer to the source (in this case it is separated by only 0.1 mm of adventitia, as opposed to 0.9 mm of mucosa and submucosa in the case of illumination from the mucosa). Since the absorption of oxygenated hemoglobin at 630 nm is lower than that of free hemoglobin, these perichondrium layers, despite their blood supply, satisfy the conditions of the diffusion approximation and yield results closer to those of Monte Carlo simulation. Therefore, we can conclude that when a multilayered organ contains layers with a high absorption coefficient, Monte Carlo numerical simulation is preferable for calculating the absorbed dose. In other cases, the adding-doubling method provides results close to those of Monte Carlo simulation under similar illumination conditions.

Results of mathematical modeling of light propagation in a colon model

Tables 12 and 13 show the simulation results for the three-layer model of the colon wall.

Tables 12 and 13 shows that Monte Carlo simulations have a higher contrast between the recorded parameters of diffusely reflected and diffusely transmitted radiation for illumination from the mucosa and muscle compared to the adding-doubling simulations for a wavelength of 532 nm, while the opposite is true for 630 nm. Regardless of the simulation type, we see that the proportion of absorbed radiation is higher for illumination from the mucosa, which is clearly related to the fact that the more or less absorbing layer is located first in the path of the incident radiation, as it receives the higher radiation dose. However, the question is not what the total absorbed dose is across layers, but rather which layer is the focus of interest. If we consider the absorption by layers when illuminated with collimated light, then when illuminated at 630 nm from the mucosa, the mucosa will receive 0.146 of the total radiation, the submucosa 0.129, and the muscle 0.048. When illuminated at the same wavelength from the muscle side, the mucosa will absorb in fractions of 0.065, the submucosa 0.070, and the muscle 0.074. Thus, the best illumination option depends on the problem statement, since in the case of a neoplasm in the mucosal layer, it is logical to irradiate from this side, and in the presence of invasion into the muscle layer, we see that greater uniformity of the absorbed dose will be achieved when illuminating from this side.

During comparison of the absorbed radiation values for the trachea and colon models obtained using the Monte Carlo and adding-doubling methods, it was found that the methods considered show agreement with an accuracy of 95±3% (95±3% for the diffuse beam and 94±3% for the collimated beam).

Таблица 11
Результаты моделирования распространения излучения с длиной волны 630 нм в шестислойной модели трахеи

Table 11
Results of modeling the propagation of radiation with a wavelength of 630 nm in a six-layer model of the trachea

StO_2	Направление Direction		MC	MC	A-D	MC	A-D
			NA 0.37	диффузный diffuse		коллимированный collimated	
Оксигенированная надхрящница Oxygenated perichondrium	со стороны слизистой from the mucosa	R_d	0.352	0.405	0.413	0.350	0.381
		A	0.577	0.537	0.503	0.578	0.526
		T_d	0.071	0.058	0.084	0.071	0.093
	со стороны адвентиции from the adventitia	R_d	0.304	0.346	0.402	0.303	0.37
		A	0.567	0.549	0.512	0.567	0.535
		T_d	0.129	0.105	0.086	0.130	0.095
Дезоксигенированная надхрящница Deoxygenated perichondrium	со стороны слизистой from the mucosa	R_d	0.351	0.404	0.408	0.349	0.376
		A	0.580	0.539	0.509	0.581	0.533
		T_d	0.069	0.057	0.083	0.069	0.091
	со стороны адвентиции from the adventitia	R_d	0.298	0.340	0.402	0.297	0.369
		A	0.575	0.558	0.513	0.576	0.538
		T_d	0.127	0.103	0.085	0.127	0.093

Таблица 12
Результаты моделирования распространения излучения с длиной волны 532 нм в трехслойной модели стенки толстого кишечника

Table 12
Results of modeling the propagation of radiation at a wavelength of 532 nm in a three-layer model of the colonic wall

		MC	MC	A-D	MC	A-D
		NA 0.37	диффузный diffuse		коллимированный collimated	
со стороны слизистой from the mucosa	R_d	0.277	0.325	0.289	0.276	0.252
	A	0.684	0.643	0.632	0.685	0.66
	T_d	0.039	0.031	0.079	0.039	0.088
со стороны мышцы from the muscle	R_d	0.228	0.282	0.287	0.226	0.249
	A	0.676	0.643	0.637	0.677	0.666
	T_d	0.096	0.076	0.076	0.097	0.085

Таблица 13
Результаты моделирования распространения излучения с длиной волны 635 нм в трехслойной модели стенки толстого кишечника

Table 13
Results of modeling the propagation of radiation at a wavelength of 635 nm in a three-layer model of the colonic wall

		MC	MC	A-D	MC	A-D
		NA 0.37	диффузный diffuse		коллимированный collimated	
со стороны слизистой from the mucosa	R_d	0.471	0.514	0.457	0.470	0.425
	A	0.323	0.312	0.282	0.323	0.293
	T_d	0.206	0.174	0.261	0.206	0.282
со стороны мышцы from the muscle	R_d	0.484	0.544	0.543	0.482	0.509
	A	0.208	0.189	0.175	0.209	0.184
	T_d	0.308	0.267	0.282	0.309	0.307

Conclusion

Comparing Monte Carlo and adding-doubling methods for modeling light transport in multilayer biological tissues has great significance for the biomedical application of calculating the absorbed dose of laser radiation during various types of laser-induced therapies, such as hyperthermia or photodynamic therapy. These modeling methods represent fundamentally different approaches to solving the radiation transport problem. By comparing the results of Monte Carlo with those of the adding-doubling method in the same multilayer configuration, the numerical accuracy of the latter's implementations can be verified and the errors introduced by its assumptions can be quantified. The adding-doubling method uses an analytical approximation of radiation transfer theory, enabling rapid calculation of the required transmission, reflection, and absorption parameters. Monte Carlo, as a numerical simulation method, is computationally expensive but can naturally handle complex 3D geometries, heterogeneous layers, and arbitrary source and detector configurations.

In this article, we compared various implementations of these two methods for multilayer models of biological tissues such as the tracheal wall (with progressively more complex structure in the models) and the colon wall. We examined the influence of the illumination side of the multilayer tissue on the light propagation parameters, the effect of thin but blood-filled layers on light propagation, and the effect of the degree of blood oxygen saturation in the tissues. We demonstrated that for multilayer media with inclusions of layers containing blood at a such concentration that the absorption coefficient and the reduced scattering coefficient become sufficiently close that the assumptions of the diffusion approximation of radiative transfer theory do not satisfy the conditions for light propagation, the use of Monte Carlo numerical simulation is preferable for calculating the absorbed dose, while in other cases the adding-doubling method yields values of absorbed dose close to Monte Carlo results under similar illumination conditions.

The work was funded by the Russian Science Foundation, grant No. 25-25-00516.

REFERENCES

1. Star W.M. Light dosimetry in vivo. *Physics in medicine and biology,* 1997, vol. 42, pp. 763–787. doi: 10.1088/0031-9155/42/5/003
2. Wilson B.C., Lilge L., Weersink R.A., Pires L. Photodynamic therapy dosimetry: current status and the emerging challenge of immune stimulation. *Journal of biomedical optics,* 2025, vol. 30, pp. S34118. doi: 10.1117/1.JBO.30.S3.S34118
3. Bergmann F., Foschum F., Marzel L., Kienle A. Ex Vivo Determination of Broadband Absorption and Effective Scattering Coefficients of Porcine Tissue. *Photonics,* 2021, vol. 8, pp. 365. https://doi.org/10.3390/photonics8090365
4. Deyev S., Lebedenko E. Targeted Bifunctional Proteins and Hybrid Nanoconstructs for Cancer Diagnostics and Therapies. *Molecular Biology,* 2017, vol. 51, pp. 788-803. doi: 10.1134/S002689331706005X
5. Albraim S., Issa H., Alaissamy K., Bartoli A., Alhabeel M. Photodynamic Therapy in Skin Treatment. *Journal of MAR Dental Sciences,* 2022, vol. 7, p. 3.
6. Serebryakova I., Surkov Yu., Fashchevskii A., Xu Y., Xia Q., Li D., Zhu D., Genina E., Tuchin V. Monte Carlo simulation of light distribution in multilayer biological tissue. *Chinese-Russian workshop on biophotonics and biomedical optics-2024,* 2024, vol. 1, pp. 33-38. doi: 10.24412/cl-37303-2024-1-33-38
7. Savelieva T.A., Krivetskaya A.A., Kustov D.M., Klobukov M.I., Romanishkin I.D., Linkov K.G., Levkin V.V., Kharnas S.S., Loschenov V.B. Application of the Kubelka-Munk model for fast intraoperative analysis of intestinal optical properties using a fiber optic spectrometer. *Biomedical Photonics,* 2025, vol. 14, pp. 30-38. doi: 10.24931/2413-9432-2025-14-3-30-38
8. Romanishkin I.D., Savelieva T.A., Ospanov A., Kalyagina N.A., Krivetskaya A.A., Udeneev A.M., Linkov K.G., Goryajnov S.A., Shugay S.V., Pavlova G.V., Pronin I.N., Loschenov V.B. Comparison of optical-spectral characteristics of glioblastoma at intraoperative diagnosis and ex vivo optical biopsy. *Biomedical Photonics,* 2024, vol. 13, pp. 4-12. doi: 10.24931/2413-9432-2024-13-4-4-12
9. Fredriksson I., Larsson M., Strömberg T. Inverse Monte Carlo method in a multilayered tissue model for diffuse reflectance spectroscopy. *J. Biomed. Opt,* 2012, vol. 17, pp. 047004. doi: 10.1117/1.JBO.17.4.047004
10. Privalov V.E., Seteikin A.Yu., Fotiadi A.E. Simulation of laser radiation propagation in inhomogeneous media with complex geometry. *Научно-технические ведомости Санкт-Петербургского государственного политехнического университета. Физико-математические науки,* 2013, vol. 4-2, pp. 148-153.
11. Liu Q., Ramanujam N. Scaling method for fast Monte Carlo simulation of diffuse reflectance spectra from multilayered turbid media. *J. Opt. Soc. Am. A,* 2007, vol. 24, pp. 1011-1025.
12. Prahl S.A., van Gemert M.J.C., Welch A.J. Determining the optical properties of turbid media by using the adding–doubling method. *Appl. Opt,* 1993, vol. 32, pp. 559-568.
13. Prahl S.A. The Adding-Doubling Method. In: Welch A. J., Van Gemert M. J. C., eds. Optical-Thermal Response of Laser-Irradiated Tissue. *Lasers, Photonics, and Electro-Optics,* Springer, Boston, MA; 1995. doi: 10.1007/978-1-4757-6092-7_5
14. Vincely V.D., Vishwanath K. Lateral light losses in integrating sphere measurements: comparison of Monte-Carlo with inverse adding-doubling algorithm. *Proc. SPIE,* 2020, pp. 11231:112310G. doi: 10.1117/12.2546265
15. https://github.com/scottprahl/iadpython
16. Lee H.H., Choi M.G., Hasan T. Application of photodynamic therapy in gastrointestinal disorders: an outdated or re-emerging technique? *The Korean journal of internal medicine,* 2017, vol. 32, pp. 1–10. doi: 10.3904/kjim.2016.200
17. Tseimakh A.E., Shoykhet I.N., Tseimakh E.A., Bedyan N.K., Makarenkov A.S. Multi-course photodynamic therapy in a patient with malignant tumor of the major duodenal papilla. Clinical case. *Biomedical Photonics,* 2025, vol. 14, pp. 39-42. doi: 10.24931/2413-9432-2025-14-3-39-42;
18. Rodrigues J.A., Correia J.H. Photodynamic Therapy for Colorectal Cancer: An Update and a Look to the Future. *International Journal of Molecular Sciences,* 2023, vol. 24, pp. 12204. doi: 10.3390/ijms241512204
19. Krivetskaya A.A., Savelieva T.A., Kustov D.M., Levkin V.V., Kharnas S.S., Loschenov V.B. Automatization of planning and control of

ЛИТЕРАТУРА

1. Star W.M. Light dosimetry in vivo // Physics in medicine and biology. – 1997. – Vol. 42. – P. 763–787. doi: 10.1088/0031-9155/42/5/003.
2. Wilson B. C., Lilge L., Weersink R. A., Pires L. Photodynamic therapy dosimetry: current status and the emerging challenge of immune stimulation // Journal of biomedical optics. – 2025. – Vol. 30. – P. 34118. doi: 10.1117/1.JBO.30.S3.S34118.
3. Bergmann F., Foschum F., Marzel L., Kienle A. Ex Vivo Determination of Broadband Absorption and Effective Scattering Coefficients of Porcine Tissue // Photonics. – 2021. – Vol. 8. – P. 365. doi: 10.3390/photonics8090365.
4. Deyev S., Lebedenko E. Targeted Bifunctional Proteins and Hybrid Nanoconstructs for Cancer Diagnostics and Therapies // Molecular Biology. – 2017. – Vol. 51. – P. 788-803. doi: 10.1134/S002689331706005X.
5. Albraim S., Issa H., Alaissamy K., Bartoli A., Alhabeel M. Photodynamic Therapy in Skin Treatment // Journal of MAR Dental Sciences. – 2022. – Vol. 7. – P. 3.
6. Serebryakova I., Surkov Yu., Fashchevskii A., Xu Y., Xia Q., Li D., Zhu D., Genina E., Tuchin V. Monte Carlo simulation of light distribution in multilayer biological tissue // Китайско-российский семинар по биофотонике и биомедицинской оптике-2024. – 2024. – Vol. 1. – P. 33-38. doi: 10.24412/cl-37303-2024-1-33-38.
7. Савельева Т.А., Кривецкая А.А., Кустов Д.М., Клобуков М.И., Романишкин И.Д., Линьков К.Г., Левкин В.В., Харнас С.С., Лощенов В.Б. Применение модели Кубелки-Мунка для быстрого интраоперационного анализа оптических свойств стенки кишечника с помощью оптоволоконного спектрометра // Biomedical Photonics. –2025. –Vol. 14. – P. 30-38. doi: 10.24931/2413-9432-2025-14-3-30-38.
8. Романишкин И.Д., Савельева Т.А., Оспанов А., Калягина Н.А., Кривецкая А.А., Уденеев А.М., Линьков К.Г., Горяйнов С.А., Шугай С.В., Павлова Г.В., Пронин И.Н., Лощенов В.Б. Сравнение оптико-спектральных характеристик глиобластомы при интраоперационной диагностике и оптической биопсии *ex vivo* // Biomedical Photonics. –2024. – Vol. 13. – P. 4-12. doi: 10.24931/2413-9432-2024-13-4-4-12.
9. Fredriksson I., Larsson M., Strömberg T. Inverse Monte Carlo method in a multilayered tissue model for diffuse reflectance spectroscopy // J. Biomed. Opt. – 2012. –Vol. 17. – P. 047004. doi: 10.1117/1.JBO.17.4.047004.
10. Привалов В.Е., Сетейкин А.Ю., Фотиади А.Э. Моделирование распространения лазерного излучения в неоднородных средах со сложной геометрией. Научно-технические ведомости Санкт-Петербургского государственного политехнического университета // Физико-математические науки. – 2013. – Vol. 4-2. –P. 148-153.
11. Liu Q., Ramanujam N. Scaling method for fast Monte Carlo simulation of diffuse reflectance spectra from multilayered turbid media // J. Opt. Soc. Am. A. – 2007. – Vol. 24. – P. 1011-1025.
12. Prahl S.A., van Gemert M.J.C., Welch A.J. Determining the optical properties of turbid media by using the adding–doubling method // Appl. Opt. – 1993. – Vol. 32. – P. 559-568.
13. Prahl S.A. The Adding-Doubling Method. In: Welch A. J., Van Gemert M. J. C., eds. Optical-Thermal Response of Laser-Irradiated Tissue // Lasers, Photonics, and Electro-Optics. Springer, Boston, MA. – 1995. doi: 10.1007/978-1-4757-6092-7_5.
14. Vincely V.D., Vishwanath K. Lateral light losses in integrating sphere measurements: comparison of Monte-Carlo with inverse adding-doubling algorithm // Proc. SPIE. – 2020. – P. 11231:112310G. doi: 10.1117/12.2546265.
15. https://github.com/scottprahl/iadpython
16. Lee H.H., Choi M.G., Hasan T. Application of photodynamic therapy in gastrointestinal disorders: an outdated or re-emerging technique? // The Korean journal of internal medicine. – 2017. – Vol. 32. – P. 1–10. doi: 10.3904/kjim.2016.200.
17. Цеймах А.Е., Шойхет Я.Н., Цеймах Е.А., Бедян Н.К., Макаренков А.С. Многокурсовая фотодинамическая терапия у пациента со злокачественным новообразованием большого дуоденального сосочка. Клинический случай // Biomedical Photonics. – 2025. – Vol. 14. – P. 39-42. doi: 10.24931/2413-9432-2025-14-3-39-42.
18. Rodrigues J.A., Correia J.H. Photodynamic Therapy for Colorectal Cancer: An Update and a Look to the Future // International Journal of Molecular Sciences. – 2023. –Vol. 24. – P. 12204. doi: 10.3390/ijms241512204.
19. Кривецкая А.А., Савельева Т.А., Кустов Д.М., Левкин В.В., Харнас С.С., Лощенов В.Б. Автоматизация планирования и контроля фо-

photodynamic therapy of gastrointestinal organs. *Biomedical Photonics,* 2025, vol. 14, pp. 40-54. doi: 10.24931/2413-9432-2025-14-2-40-54

20. Singh H., Benn B.S., Jani C., Abdalla M., Kurman J.S. Photodynamic therapy for treatment of recurrent adenocarcinoma of the lung with tracheal oligometastasis. *Respiratory medicine case reports,* 2022, vol. 37, pp. 101620. doi: 10.1016/j.rmcr.2022.101620
21. Jung H.S., Kim H.J., Kim K.W. Intraoperative photodynamic therapy for tracheal mass in non-small cell lung cancer: A case report. *World journal of clinical cases,* 2023, vol. 11, pp. 3915–3920. doi: 10.12998/wjcc.v11.i16.3915
22. Martin L.K., Otterson G.A., Bekaii-Saab T. Photodynamic therapy (PDT) may provide effective palliation in the treatment of primary tracheal carcinoma: a small case series. *Photomedicine and laser surgery,* 2012, vol. 30, pp. 668–671. doi: 10.1089/pho.2012.3293
23. Hohmann M., Lengenfelder B., Kanawade R., Klämpfl F., Douplik A., Albrecht H. Measurement of optical properties of pig esophagus by using a modified spectrometer set-up. *Journal of Biophotonics,* 2017, vol. 11. doi: 10.1002/jbio.201600187
24. Descalle M.-A., Jacques S.L., Prahl S.A., Laing T.J., Martin W.R. Measurements of ligament and cartilage optical properties at 35mm, 365nm and in the visible range [440-800nm]. *SPIE,* 1998, vol. 3195, pp. 280-286.
25. Youn J.-I., Telenkov S.A., Kim E., Bhavaraju N.C., Wong B.J.F., Valvano J. W., Milner T. E. Optical and Thermal Properties of Nasal Septal Cartilage. *Lasers in Surgery and Medicine,* 2000, vol. 27, pp. 119-128.
26. Bagratashvili N.V., Sviridov A.P., Sobol E.N., Kitai M.S. Optical properties of nasal septum cartilage. *Proc. SPIE,* 1998, vol. 3254. doi: 10.1117/12.308189
27. Nawn C.D., Blackburn M.B., De Lorenzo R.A., Ryan K.L. Using spectral reflectance to distinguish between tracheal and oesophageal tissue: applications for airway management. *Anaesthesia,* 2019, vol. 74, pp. 340-347. doi: 10.1111/anae.14566
28. Ebert D., Roberts C., Farrar S., Johnston W., Litsky A., Bertone A. Articular Cartilage Optical Properties in the Spectral Range 300-850 nm. *Journal of biomedical optics,* 1998, vol. 3, pp. 326-33. doi: 10.1117/1.429893
29. Khan R., Gul B., Khan S., Nisar H., Ahmad I. Refractive index of biological tissues: Review, measurement techniques, and applications. *Photodiagnosis and photodynamic therapy,* 2021, vol. 33, pp. 102192. doi: 10.1016/j.pdpdt.2021.102192
30. Carvalho S., Gueiral N., Nogueira E., Henrique R., Oliveira L., Tuchin V. Wavelength dependence of the refractive index of human colorectal tissues: comparison between healthy mucosa and cancer. *Journal of Biomedical Photonics & Engineering,* 2016, vol. 2, pp. 040307-1. doi: 10.18287/JBPE16.02.040307
31. Wiesner W., Mortelé K. J., Ji H., Ros P. R. Normal colonic wall thickness at CT and its relation to colonic distension. *Journal of computer assisted tomography,* 2002, vol. 26, pp. 102–106. doi: 10.1097/00004728-200201000-00015
32. Wei H.J., Xing D., Lu J.J., Gu H.M., Wu G.Y., Jin Y. Determination of optical properties of normal and adenomatous human colon tissues in vitro using integrating sphere techniques. *World journal of gastroenterology,* 2005, vol. 11, pp. 2413–2419. doi: 10.3748/wjg.v11.i16.2413
33. Wei H., Xing D., Wu G., Gu H., Lu J., Jin Y., Li X.-Y. Differences in optical properties between healthy and pathological human colon tissues using a Ti:sapphire laser: an in vitro study using the Monte Carlo inversion technique. *J. Biomed. Opt,* 2005, vol. 10, pp. 044022. doi: 10.1117/1.1990125
34. Bashkatov A., Genina E., Kochubey V., Rubtsov V., Kolesnikova E., Tuchin V. Optical properties of human colon tissues in the 350–2500 nm spectral range. *Quantum Electronics,* 2014, vol. 44, pp. 77. doi: 10.1070/QE2014v044n08ABEH015613
35. Carvalho S., Gueiral N., Nogueira E., Henrique R., Oliveira L., Tuchin V. V. Comparative study of the optical properties of colon mucosa and colon precancerous polyps between 400 and 1000 nm. *Proc. SPIE,* 2017, pp. 10063:100631L. doi: 10.1117/12.2253023
36. Vo-Dinh T., ed. *Biomedical Photonics Handbook,* 1st ed. CRC Press; 2003. doi: 10.1201/9780203008997
37. Ismael F.S., Amasha H.M., Bachir W.H. A diffusion equation based algorithm for determination of the optimal number of fibers used for breast cancer treatment planning in photodynamic therapy. *Biomedical Photonics,* 2019, vol. 8, pp. 17-27. doi: 10.24931/2413-9432-2019-8-4-17-27

тодинамической терапии органов желудочно-кишечного тракта // Biomedical Photonics. – 2025. – 14. – P. 40-54. doi: 10.24931/2413-9432-2025-14-2-40-54.

20. Singh H., Benn B.S., Jani C., Abdalla M., Kurman J.S. Photodynamic therapy for treatment of recurrent adenocarcinoma of the lung with tracheal oligometastasis // Respiratory medicine case reports. – 2022. – Vol. 37. – P. 101620. doi: 10.1016/j.rmcr.2022.101620.
21. Jung H.S., Kim H.J., Kim K.W. Intraoperative photodynamic therapy for tracheal mass in non-small cell lung cancer: A case report // World journal of clinical cases. – 2023. – Vol. 11. – P. 3915–3920. https://doi.org/10.12998/wjcc.v11.i16.3915.
22. Martin L.K., Otterson G.A., Bekaii-Saab T. Photodynamic therapy (PDT) may provide effective palliation in the treatment of primary tracheal carcinoma: a small case series // Photomedicine and laser surgery. – 2012. – Vol. 30. – P. 668–671. doi: 10.1089/pho.2012.3293.
23. Hohmann M., Lengenfelder B., Kanawade R., Klämpfl F., Douplik A., Albrecht H. Measurement of optical properties of pig esophagus by using a modified spectrometer set-up // Journal of Biophotonics. – 2017. – Vol. 11. doi: 10.1002/jbio.201600187.
24. Descalle M.-A., Jacques S.L., Prahl S.A., Laing T.J., Martin W.R. Measurements of ligament and cartilage optical properties at 35mm, 365nm and in the visible range [440-800nm] // SPIE. – 1998. – Vol. 3195. – P. 280-286.
25. Youn J.-I., Telenkov S. A., Kim E., Bhavaraju N. C., Wong B. J. F., Valvano J. W., Milner T. E. Optical and Thermal Properties of Nasal Septal Cartilage // Lasers in Surgery and Medicine. – 2000. – Vol. 27. – P. 119-128.
26. Bagratashvili N.V., Sviridov A.P., Sobol E.N., Kitai M.S. Optical properties of nasal septum cartilage // Proc. SPIE. – 1998. – P.3254. https://doi.org/10.1117/12.308189.
27. Nawn C.D., Blackburn M.B., De Lorenzo R.A., Ryan K.L. Using spectral reflectance to distinguish between tracheal and oesophageal tissue: applications for airway management // Anaesthesia. – 2019. – Vol. 74. – P. 340-347. doi: 10.1111/anae.14566.
28. Ebert D., Roberts C., Farrar S., Johnston W., Litsky A., Bertone A. Articular Cartilage Optical Properties in the Spectral Range 300-850 nm // Journal of biomedical optics. – 1998. – Vol. 3. – P. 326-33. doi: 10.1117/1.429893.
29. Khan R., Gul B., Khan S., Nisar H., Ahmad I. Refractive index of biological tissues: Review, measurement techniques, and applications // Photodiagnosis and photodynamic therapy. – 2021. – Vol. 33. – P. 102192. doi: 10.1016/j.pdpdt.2021.102192.
30. Carvalho S., Gueiral N., Nogueira E., Henrique R., Oliveira L., Tuchin V. Wavelength dependence of the refractive index of human colorectal tissues: comparison between healthy mucosa and cancer // Journal of Biomedical Photonics & Engineering. – 2016. – Vol. 2. – P. 040307-1. doi: 10.18287/JBPE16.02.040307.
31. Wiesner W., Mortelé K.J., Ji H., Ros P.R. Normal colonic wall thickness at CT and its relation to colonic distension // Journal of computer assisted tomography. – 2002. – Vol. 26. – P. 102–106. doi: 10.1097/00004728-200201000-00015.
32. Wei H.J., Xing D., Lu J.J., Gu H.M., Wu G.Y., Jin Y. Determination of optical properties of normal and adenomatous human colon tissues in vitro using integrating sphere techniques // World journal of gastroenterology. – 2005. – Vol. 11. – P. 2413–2419. doi: 10.3748/wjg.v11.i16.2413.
33. Wei H., Xing D., Wu G., Gu H., Lu J., Jin Y., Li X.-Y. Differences in optical properties between healthy and pathological human colon tissues using a Ti:sapphire laser: an in vitro study using the Monte Carlo inversion technique // J. Biomed. Opt. – 2005. – Vol. 10. – P. 044022. doi: 10.1117/1.1990125.
34. Bashkatov A., Genina E., Kochubey V., Rubtsov V., Kolesnikova E., Tuchin V. Optical properties of human colon tissues in the 350–2500 nm spectral range // Quantum Electronics. – 2014. – Vol. 44. – P. 77. doi: 10.1070/QE2014v044n08ABEH015613.
35. Carvalho S., Gueiral N., Nogueira E., Henrique R., Oliveira L., Tuchin V.V. Comparative study of the optical properties of colon mucosa and colon precancerous polyps between 400 and 1000 nm // Proc. SPIE. – 2017. – P. 10063:100631L. doi: 10.1117/12.2253023.
36. Vo-Dinh T., ed. Biomedical Photonics Handbook. 1st ed. CRC Press. – 2003. doi: 10.1201/9780203008997.
37. Ismael F.S., Amasha H.M., Bachir W.H. Алгоритм определения оптимального числа волокон используемых при внутритканевой фотодинамической терапии рака молочной железы на основании диффузионного уравнения // Biomedical Photonics. – 2019. – Vol. 8. – P. 17-27. doi: 10.24931/2413-9432-2019-8-4-17-27

SECONDARY LYMPHEDEMA AS A COMPLICATION OF SURGICAL TREATMENT FOR BREAST CANCER: AUTOTRANSPLANTATION OF LYMPH NODES USING ICG LYMPHOGRAPHY

Troshenkov E.A., Polyak M.A., Shakhbanova K.A., Kaprin A.D., Filonenko E.V., Kutsuradis A.F., Mantaridis D.
National Medical Research Center of Radiology of Ministry of Health of Russia, Moscow, Russia

Abstract

Secondary upper limb lymphedema remains one of the most significant complications of surgical and radiation treatment of breast cancer and is characterized by progressive impairment of lymphatic drainage, chronic inflammation, and soft tissue fibrosis. In cases of pronounced anatomical and functional damage to lymphatic collectors, the effectiveness of conservative therapy and lymphovenous anastomoses is limited, necessitating the use of physiological microsurgical reconstruction techniques. Vascularized lymph node transfer (VLNT) is considered a pathogenetically substantiated approach to restoring lymphatic drainage, combining the mechanical «lymphatic pump» effect with stimulation of lymphangiogenesis through growth factor secretion. Imaging modalities of the lymphatic system, including indocyanine green (ICG) lymphography and lymphoscintigraphy, play a crucial role in patient selection and in the assessment of surgical outcomes by enabling visualization of dermal backflow, collector obliteration, and the formation of new lymphatic pathways. The paper presents a clinical case of a patient with stage IIA lymphedema following comprehensive breast cancer treatment, in whom the absence of clinical improvement after lymphovenous bypass served as an indication for delayed breast reconstruction with a free DIEP flap combined with inguinal vascularized lymph node transfer. Postoperative follow-up demonstrated a reduction in limb volume, decreased dermal backflow, and the appearance of linear lymphatic flow patterns in the transplant area. These findings confirm the potential of vascularized lymph node transfer as a component of a comprehensive surgical strategy for the treatment of secondary lymphedema in patients after combined breast cancer therapy.

Key words: lymphedema, breast cancer, lymph node transfer, ICG lymphography, microsurgery

Contacts: Polyak M.A., e-mail: marianna29@yandex.ru

For citations: Troshenkov E.A., Polyak M.A., Shakhbanova K.A., Kaprin A.D., Filonenko E.V., Kutsuradis A.F., Mantaridis D. Secondary lymphedema as a complication of surgical treatment for breast cancer: autotransplantation of lymph nodes using ICG lymphography, *Biomedical Photonics*, 2026, vol. 15, no. 1, pp. 30–36. doi: 10.24931/2413–9432–2026–15-1-30-36

ВТОРИЧНАЯ ЛИМФЕДЕМА КАК ОСЛОЖНЕНИЕ ХИРУРГИЧЕСКОГО ЛЕЧЕНИЯ РАКА МОЛОЧНОЙ ЖЕЛЕЗЫ: АУТОТРАНСПЛАНТАЦИИ ЛИМФАТИЧЕСКИХ УЗЛОВ С ИСПОЛЬЗОВАНИЕМ ICG-ЛИМФОГРАФИИ

Е.А. Трошенков, М.А. Поляк, К.А. Шахбанова, А.Д. Каприн, Е.В. Филоненко, А.Ф. Куцурадис, Д. Мантаридис
Национальный медицинский исследовательский центр радиологии Минздрава России, Москва, Россия

Резюме

Вторичная лимфедема верхней конечности остаётся одним из наиболее значимых осложнений хирургического и лучевого лечения рака молочной железы и характеризуется прогрессирующим нарушением лимфатического оттока, развитием хронического воспаления и фиброза мягких тканей. При выраженных анатомо-функциональных изменениях лимфатических коллекторов эффективность консервативной терапии и лимфовенозных анастомозов ограничена, что определяет необходимость применения физиологических микрохирургических методов реконструкции. Аутотрансплантация васкуляризованных лимфатических узлов рассматривается как патогенетически обоснованный способ восстановления лимфодренажа, сочетающий механический эффект «лимфатического насоса»

и стимуляцию лимфангиогенеза за счёт секреции факторов роста. Существенную роль в отборе пациенток и оценке эффективности вмешательства играют методы визуализации лимфатической системы, включая ICG-лимфографию и лимфосцинтиграфию, позволяющие выявлять дермальный рефлюкс, облитерацию коллекторов и формирование новых путей лимфатического транспорта. В работе представлено клиническое наблюдение пациентки с лимфедемой IIA стадии после комплексного лечения рака молочной железы, у которой отсутствие эффекта от лимфовенозного шунтирования послужило основанием для выполнения отсроченной реконструкции молочной железы свободным DIEP-лоскутом в сочетании с трансплантацией паховых лимфатических узлов. В послеоперационном периоде отмечено уменьшение объёма конечности, снижение выраженности дермального рефлюкса и появление линейных участков лимфатического транспорта в зоне трансплантата. Полученные данные подтверждают перспективность трансплантации васкуляризованных лимфатических узлов как компонента комплексной хирургической стратегии лечения вторичной лимфедемы у пациенток после комбинированного лечения рака молочной железы.

Ключевые слова: лимфедема, рак молочной железы, трансплантация лимфатических узлов, ICG-лимфография, микрохирургия.

Контакты: Поляк М.А., e-mail: marianna29@yandex.ru

Для цитирования: Трошенков Е.А., Поляк М.А., Шахбанова К.А., Каприн А.Д., Филоненко Е.В., Куцурадис А.Ф., Мантаридис Д. Вторичная лимфедема как осложнение хирургического лечения рака молочной железы: аутотрансплантации лимфатических узлов с использованием ICG-лимфографии // Biomedical Photonics. – 2026. –Т. 15, № 1. – С. 30–36. doi: 10.24931/2413–9432–2026–15-1-30-36

Introduction

Lymphedema is a chronic disease caused by impaired lymphatic transport and characterized by the accumulation of protein-rich fluid in the interstitial space, followed by chronic inflammation, fibrosis, and structural remodeling of soft tissues [1]. According to the literature, lymphedema is considered a dynamic pathological process that includes not only mechanical obstruction of the lymphatic pathways but also complex immune-inflammatory changes leading to progressive tissue remodeling [2].

Upper extremity lymphedema following breast cancer surgery remains one of the most significant challenges in modern oncology and reconstructive surgery. Despite the introduction of sentinel lymph node biopsy and the de-escalation of axillary surgery, the incidence of lymphedema after axillary lymph node dissection remains high, reaching 40% [3]. Additional risk factors include radiation therapy, a high body mass index, infectious complications (recurrent episodes of erysipelas or cellulitis), and the extent of surgical intervention [2].

The development of lymphedema leads to a significant decrease in the patient's quality of life, limited upper limb function, chronic pain, and an increased risk of infectious complications, making this problem not only medically but also socially significant [4].

A modern approach to treating lymphedema involves a stepwise approach. In the early stages, the leading method remains comprehensive physical anti-edema therapy, including compression therapy, manual lymphatic drainage, exercise therapy, and meticulous skin care [5]. However, with the development of severe fibrotic changes and destruction of lymphatic collectors, the effectiveness of conservative therapy is significantly reduced, necessitating the use of surgical correction methods [6].

The development of microvascular surgery has led to the introduction of physiological methods for reconstructing lymphatic drainage—lymphatic venous anastomoses (LVA) and vascularized lymph node autotransplantation (VLNT). LVA is most effective in the early stages of the disease when lymphatic vessels are preserved, while VLNT is considered the preferred method for severe anatomical and functional changes and the development of fibrosis, providing both mechanical restoration of lymphatic drainage and the potential lymphangiogenic effect of transplanted nodes [7].

Thus, the search for optimal surgical tactics for the treatment of secondary lymphedema after breast cancer surgery remains a *relevant task* of modern oncomammology and reconstructive surgery. This article presents a clinical case of vascularized lymph node autotransplantation and reviews the current literature on this topic.

Technical Aspects and Mechanisms of Effectiveness of Vascularized Lymph Node Transplantation

Autotransplantation of vascularized lymph nodes is a physiological microsurgical method for reconstructing lymphatic drainage and is used in secondary lymphedema, primarily in cases of severe anatomical and functional changes in the lymphatic system. This technique involves isolating a block of lymph nodes with surrounding adipose tissue and feeding arterial and venous vessels, forming a vascular pedicle, followed by transferring the flap to the lymphedema area and performing microsurgical arterial and venous anastomoses [8].

The most commonly used donor sites are the inguinal region, as well as the axillary, omental, submental, lateral thoracic, supraclavicular, and cervical regions [9]. The choice of donor site is determined by anatomical

features, the required tissue volume, and the risk of developing donor lymphedema.

Considering that secondary lymphedema of the upper limb most often develops after axillary lymph node dissection combined with radiation therapy, a pronounced fibrous scarring process often develops in the recipient site. Preparation of the graft bed is a fundamentally important stage of the surgery and includes excision of fibrous tissue, decompression of vascular and nerve structures, and creation of conditions for neoangiogenesis and lymphangiogenesis. Removal of scar tissue reduces mechanical compression and eliminates the barrier to the formation of new lymphatic collaterals [10].

Transplantation is performed by placing the vascularized lymphatic complex into the prepared bed and fixing it with soft tissue. Vascular anastomoses of arteries and veins are performed microsurgically, ensuring the restoration of blood flow and integration of the graft into the lymphatic system of the limb [11].

The clinical effect of autotransplantation of vascularized lymph nodes is achieved through several complementary mechanisms.

The first theory, the so-called "lymphatic pump" or pressure gradient concept, suggests that the transplanted lymphatic complex functions as a zone of reduced interstitial pressure. Active blood flow within the graft creates conditions for passive lymphatic influx from surrounding tissues, which ensures early reduction of edema in the postoperative period [12].

The second theory involves the induction of lymphangiogenesis. Experimental and clinical studies have shown that transplanted lymph nodes are capable of secreting vascular endothelial growth factor-C (VEGF-C), which stimulates the proliferation of lymphatic endothelial cells and the formation of new lymphatic collectors. Thus, new lymphatic drainage pathways and lymphovenous connections are formed in the long-term period [13].

The functional activity of the graft is confirmed by instrumental methods. Lymphography using indocyanine green (ICG) and lymphoscintigraphy demonstrate a redistribution of lymphatic flow to the graft area already in the early postoperative period, followed by the formation of new lymphatic collaterals and improved drainage function of the limb [12].

Thus, vascularized lymph node transplantation represents a pathogenetically substantiated method for the surgical correction of secondary lymphedema, combining mechanical, angiogenic, and immunomodulatory effects.

Indications and Contraindications for Vascularized Lymph Node Transplantation

The choice of vascularized lymph node transplantation as a treatment for lymphedema is based on the stage of the disease, the severity of structural changes in the lymphatic system, and the results of previous conservative therapy. This method is primarily considered for patients with stage II-III lymphedema according to the International Society of Lymphology (ISL) classification, in whom conservative therapy has failed to achieve a stable functional result [14].

The key selection criterion is the presence of anatomical and functional failure of the lymphatic collectors, confirmed by instrumental methods (ICG lymphography, lymphoscintigraphy), with signs of severe dermal reflux, segmental vascular obliteration, or complete vascular destruction. In such cases, performing lymphovenous anastomoses is technically difficult or impractical, which justifies the choice of lymph node transplantation as a pathogenetically targeted reconstruction method.

The main indications for vascularized lymph node transplantation include:

- ISL stage II-III lymphedema with severe soft tissue fibrosis;
- lack of clinically significant effect from adequate conservative therapy;
- recurrent episodes of cellulitis (erysipelas);
- obliteration or a sharp decrease in the number of functioning lymphatic vessels;
- severe pain, decreased limb function, and a significant deterioration in quality of life.

An additional factor in favor of surgical treatment may be disease progression despite adherence to a compression regimen and rehabilitation measures.

Contraindications to vascularized lymph node transplantation can be divided into absolute and relative. This approach allows this intervention to be considered not as a universal method, but as a component of a personalized surgical strategy for the treatment of secondary lymphedema.

Absolute contraindications include:

- local recurrence of breast cancer or progression of the oncological disease;
- the presence of distant metastases.

Relative contraindications include:

- severe microcirculation disorders in the recipient site (post-radiation vasculitis, critically reduced perfusion);
- severe forms of neuropathy or neuritis of the brachial plexus, limiting the possibility of full postoperative rehabilitation;
- lack of suitable recipient vessels for the formation of microsurgical anastomoses;
- severe somatic diseases that increase the risk of microsurgical intervention.

Thus, indications for VLNT are determined based on a comprehensive assessment of the stage of lymphedema, instrumental imaging data, the effectiveness of

conservative treatment, and the patient's oncological status. Optimal patient selection is a key factor in achieving a sustainable clinical outcome [15, 16].

Clinical Observation

A 49-year-old female patient presented to the P.A. Herzen Moscow Oncology Research Institute – a branch of the National Medical Research Center of Radiology of the Ministry of Health of Russia with a diagnosis of stage IIIC right breast cancer, pT2N3aM0, luminal type A, status after combined treatment in 2023 (05.08.2023 – right radical mastectomy, 4 cycles of neoadjuvant chemotherapy according to the DC regimen from 28.08.2023 to 01.11.2023, external beam radiotherapy from 21.11.2023 to 26.12.2023, total focal dose 50 Gy).

From the medical history, it is known that after completion of the combined treatment for the primary disease, the patient began to notice increasing swelling of the right upper limb. The patient did not wear a compression sleeve, as a result of which the swelling became persistent.

At the A.F. Tsyb Medical Radiological Research Center – a branch of the National Medical Research Center of Radiology of the Ministry of Health of Russia, on 15.02.2024 and 02.05.2024, lymphovenous bypasses of the right upper limb were performed: at the level of the forearm and the hand, respectively.

Despite surgical interventions, conservative therapy, and wearing of compression garments, the desired effect on swelling was not achieved. Furthermore, the patient noted a significant decrease in quality of life due to the absence of a breast.

The patient was referred to the P.A. Herzen Moscow Oncology Research Institute for further evaluation and determination of treatment strategies for secondary

Рис. 1. Внешний вид правой верхней конечности до начала лечения. Лимфедема IIA стадии по классификации ISL.
Fig. 1. Clinical appearance of the right upper limb before treatment. Stage IIA lymphedema according to the ISL classification.

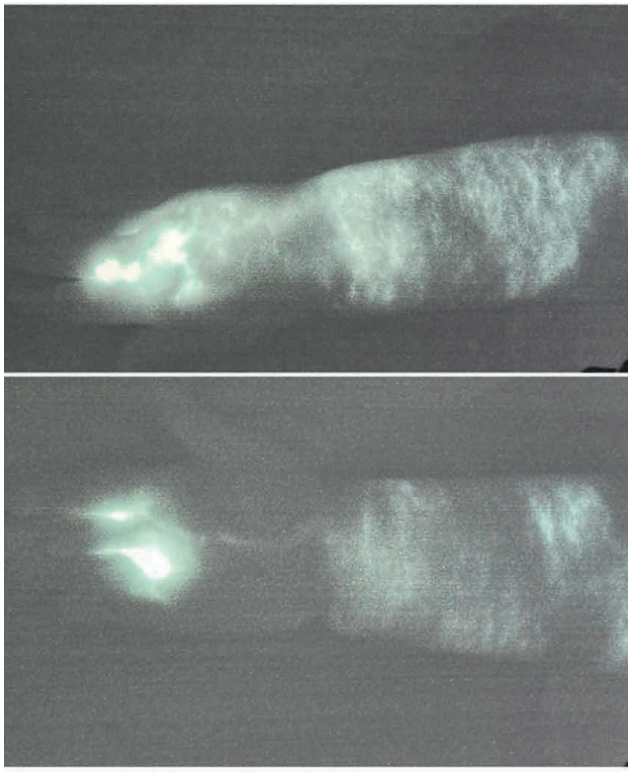

Рис. 2. ICG-лимфография правой верхней конечности до лечения: выраженный дермальный рефлюкс, отсутствие линейных лимфатических коллекторов в проксимальных отделах.
Fig. 2. ICG lymphography of the right upper limb before treatment: pronounced dermal backflow and absence of linear lymphatic collectors in the proximal segments.

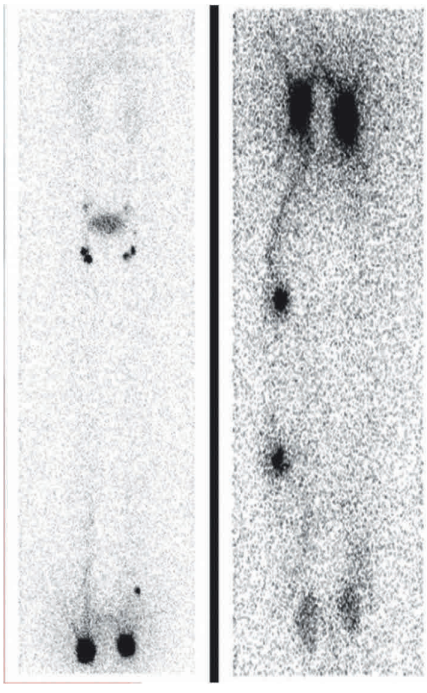

Рис. 3. Лимфосцинтиграфия правой верхней конечности: лимфатический транспорт замедлен, регионарные подмышечные узлы не визуализируются.
Fig. 3. Lymphoscintigraphy of the right upper limb: lymphatic flow is slowed, and regional axillary nodes are not visualized.

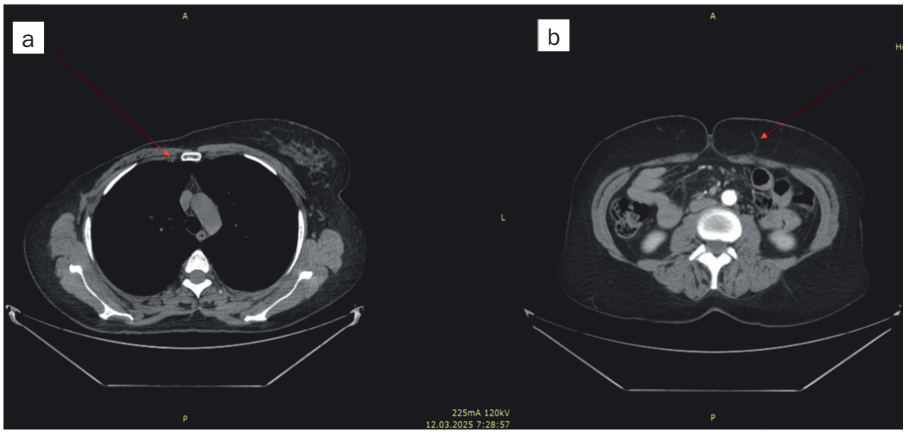

Рис. 4. КТ-ангиография для планирования микрохирургической реконструкции: a – передняя брюшная стенка: виден перфорант глубокой нижнеэпигастральной артерии для выделения сосудистой ножки; b – грудная клетка со стороны ранее выполненной мастэктомии: сохранные внутригрудные сосуды, пригодные для реконструкции.
Fig. 4. CT angiography for microsurgical reconstruction planning: a – anterior abdominal wall: perforator of the deep inferior epigastric artery visible for harvesting the vascular pedicle; b – chest on the side of prior mastectomy: preserved intrathoracic vessels suitable for reconstruction.

lymphedema and the possibility of right breast reconstruction.

On examination: the right upper extremity was enlarged, primarily in the forearm and shoulder area, with moderate fibrotic changes in the soft tissues and decreased skin elasticity. The lymphedema corresponded to stage IIA according to the ISL classification.

According to ICG lymphography data, pronounced dermal reflux, the absence of formed linear lymphatic collectors in the proximal parts of the limb and signs of failure of previously performed lymphovenous anastomoses were revealed.

Lymphoscintigraphy confirmed a significant slowdown in lymphatic transport and lack of visualization of regional axillary lymph nodes.

CT angiography visualized a perforator of the deep inferior epigastric artery on the anterior abdominal wall, necessary for isolating the vascular pedicle, as well as preserved intrathoracic vessels on the side of the previously performed mastectomy, which made it possible to plan microsurgical reconstruction.

Given the severe anatomical and functional impairment of lymphatic drainage, the lack of response to lymphovenous bypass, and the patient's desire to restore the lost breast, a decision was made to perform delayed reconstruction of the right breast using a free DIEP flap combined with vascularized inguinal lymph node transplantation.

During the surgery, after excision of scar-fibrous tissue in the axillary region, an adequate recipient bed

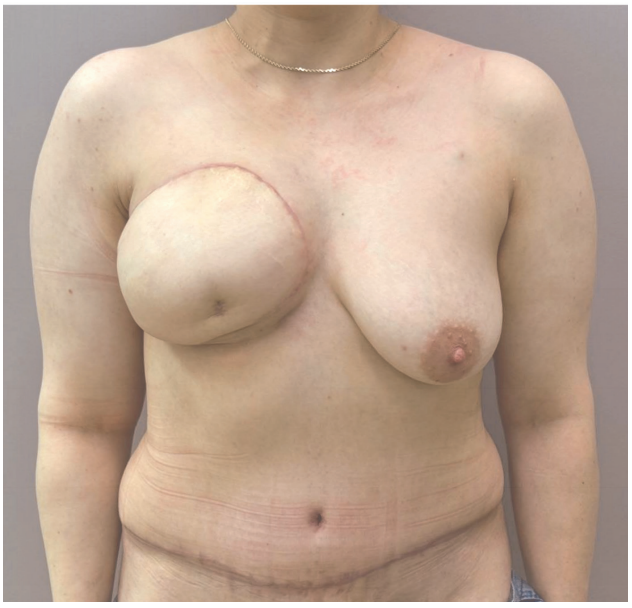

Рис. 5. Клинический осмотр через 6 мес после лечения: видна восстановленная молочная железа, уменьшение объема конечности и снижение симптомов лимфостаза.
Fig. 5. Clinical examination 6 months after treatment: reconstructed breast visible, limb volume reduced, and lymphedema symptoms improved.

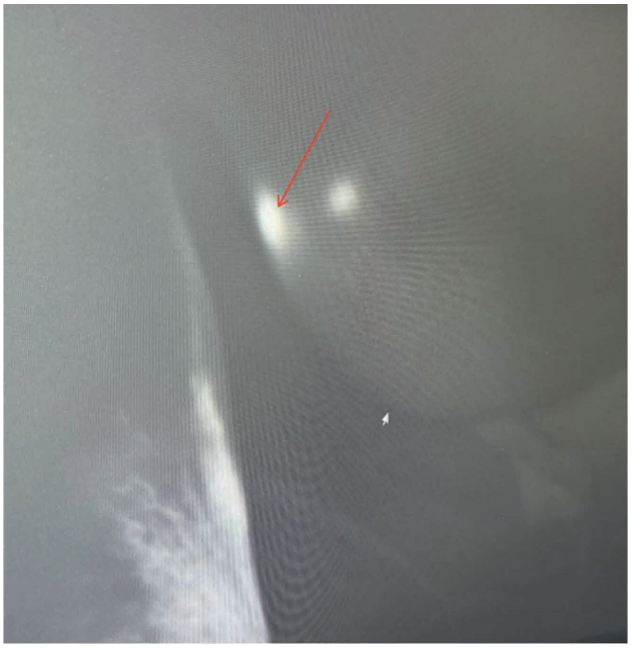

Рис. 6. ICG-лимфография после реконструкции: накопление контраста в зоне трансплантата.
Fig. 6. ICG lymphography after reconstruction: contrast accumulation in the transplant area.

was created. A DIEP flap was harvested, incorporating superficial inguinal lymph nodes on a vascular pedicle. End-to-end microvascular anastomoses were formed with the thoraco-dorsal vessels. The lymphatic component was placed orthotopically in the axillary area. No intraoperative or early postoperative complications were noted.

Six months after surgery, the patient noted a decrease in the feeling of heaviness and tension in the limb, decreased tissue density, and a reduced dependence on constant compression therapy. Follow-up ICG lymphography showed a reduction in the severity of dermal reflux and the appearance of linear areas of lymphatic transport with contrast accumulation in the transplant area. Clinically, a 2-3 cm reduction in limb circumference at the forearm level was recorded. No episodes of erysipelas were observed postoperatively.

Conclusion

Vascularized lymph node autotransplantation is a modern and highly effective microsurgical method for treating lymphedema, especially at stages characterized by destruction of lymphatic drainage and decreased effectiveness of conservative therapy. This method ensures sustainable limb volume reduction, restoration of lymphatic drainage, a reduction in the incidence of inflammatory complications, and a significant improvement in patients' quality of life. Optimization of donor site selection, the use of imaging techniques, and microsurgical techniques minimize risks and improve the effectiveness of the procedure. VLNT represents a promising tool for a comprehensive approach to lymphedema treatment, particularly in patients following comprehensive breast cancer treatment, where lymphatic system changes are most pronounced.

REFERENCES

1. Wang D., Lyons D., Skoracki R. Lymphedema: Conventional to Cutting Edge Treatment. *Semin Intervent Radiol*, 2020, Vol. 37(3), pp. 295-308. doi: 10.1055/s-0040-1713447.
2. Sharifi N., Ahmad S. Breast cancer-related lymphedema: A critical review on recent progress. *Surg Oncol*, 2024, Vol. 56, pp. 102124. doi: 10.1016/j.suronc.2024.102124.
3. Rockson S.G. Lymphedema after Breast Cancer Treatment. *N Engl J Med*, 2018, Vol. 379(20), pp. 1937-1944. doi: 10.1056/NEJMcp1803290.
4. Taghian N.R., Miller C.L., Jammallo L.S., O'Toole J., Skolny M.N. Lymphedema following breast cancer treatment and impact on quality of life: a review. *Crit Rev Oncol Hematol*, 2014, Vol. 92(3), pp. 227-234. doi: 10.1016/j.critrevonc.2014.06.004.
5. Pappalardo M., Starnoni M., Franceschini G., Baccarani A., De Santis G. Breast Cancer-Related Lymphedema: Recent Updates on Diagnosis, Severity and Available Treatments. *J Pers Med*, 2021, Vol. 11(5), pp. 402. doi: 10.3390/jpm11050402.
6. Drobot D., Zeltzer A.A. Surgical treatment of breast cancer related lymphedema-the combined approach: a literature review. *Gland Surg*, 2023, Vol. 12(12), pp. 1746-1759. doi: 10.21037/gs-23-247.
7. Kitayama S. Diagnosis and Treatments of Limb Lymphedema: Review. *Ann Vasc Dis*, 2024, Vol. 17, №2, pp. 114-119. doi: 10.3400/avd.ra.24-00011.
8. Hassani C., Tran K., Palmer S.L., Patel K.M. Vascularized Lymph Node Transfer: A Primer for the Radiologist. *Radiographics*, 2020, Vol. 40(4), pp. 1073-1089. doi: 10.1148/rg.2020190118.
9. Ozturk C.N., Ozturk C., Glasgow M., Platek M., Ashary Z., Kuhn J., Aronoff N., Lohman R., Djohan R., Gurunluoglu R. Free vascularized lymph node transfer for treatment of lymphedema: A systematic evidence based review. *J Plast Reconstr Aesthet Surg*, 2016, Vol. 69(9), pp. 1234-1247. doi: 10.1016/j.bjps.2016.06.022.
10. Senger J.B., Rajaii R., Slater C., Cho M.J. Proximal vs. Recipient Site for Vascular Lymph Node Transfers for Breast Cancer-Related Lymphedema: A Meta-Analysis and Systematic Review. *J Clin Med*, 2025, Vol. 14(20), pp. 7281. doi: 10.3390/jcm14207281.
11. Schaverien M.V., Badash I., Patel K.M., Selber J.C., Cheng M.H. Vascularized Lymph Node Transfer for Lymphedema. *Semin*

ЛИТЕРАТУРА

1. Wang D., Lyons D., Skoracki R. Lymphedema: Conventional to Cutting Edge Treatment // Semin Intervent Radiol. – 2020. – Vol. 37, №3. – P. 295-308. doi: 10.1055/s-0040-1713447.
2. Sharifi N., Ahmad S. Breast cancer-related lymphedema: A critical review on recent progress // Surg Oncol. – 2024. – Vol. 56. – P. 102124. doi: 10.1016/j.suronc.2024.102124.
3. Rockson S.G. Lymphedema after Breast Cancer Treatment // N Engl J Med. – 2018. – Vol. 379, №20. – P. 1937-1944. doi: 10.1056/NEJMcp1803290.
4. Taghian N.R., Miller C.L., Jammallo L.S., O'Toole J., Skolny M.N. Lymphedema following breast cancer treatment and impact on quality of life: a review // Crit Rev Oncol Hematol. – 2014. – Vol. 92, №3. – P. 227-234. doi: 10.1016/j.critrevonc.2014.06.004.
5. Pappalardo M., Starnoni M., Franceschini G., Baccarani A., De Santis G. Breast Cancer-Related Lymphedema: Recent Updates on Diagnosis, Severity and Available Treatments // J Pers Med. – 2021. – Vol. 11, №5. – P. 402. doi: 10.3390/jpm11050402.
6. Drobot D., Zeltzer A.A. Surgical treatment of breast cancer related lymphedema-the combined approach: a literature review // Gland Surg. – 2023. – Vol. 12, №12. – P. 1746-1759. doi: 10.21037/gs-23-247.
7. Kitayama S. Diagnosis and Treatments of Limb Lymphedema: Review // Ann Vasc Dis. – 2024. – Vol. 17, №2. – P. 114-119. doi: 10.3400/avd.ra.24-00011.
8. Hassani C., Tran K., Palmer S.L., Patel K.M. Vascularized Lymph Node Transfer: A Primer for the Radiologist // Radiographics. – 2020. – Vol. 40, №4. – P. 1073-1089. doi: 10.1148/rg.2020190118.
9. Ozturk C.N., Ozturk C., Glasgow M., Platek M., Ashary Z., Kuhn J., Aronoff N., Lohman R., Djohan R., Gurunluoglu R. Free vascularized lymph node transfer for treatment of lymphedema: A systematic evidence based review // J Plast Reconstr Aesthet Surg. – 2016. – Vol. 69, №9. – P. 1234-1247. doi: 10.1016/j.bjps.2016.06.022.
10. Senger J.B., Rajaii R., Slater C., Cho M.J. Proximal vs. Recipient Site for Vascular Lymph Node Transfers for Breast Cancer-Related Lymphedema: A Meta-Analysis and Systematic Review // J Clin Med. – 2025. – Vol. 14, №20. – P. 7281. doi: 10.3390/jcm14207281.
11. Schaverien M.V., Badash I., Patel K.M., Selber J.C., Cheng M.H. Vascularized Lymph Node Transfer for Lymphedema // Semin

Plast Surg, 2018, Vol. 32(1), pp. 28-35. doi: 10.1055/s-0038-1632401.
12. Suami H., Scaglioni M.F., Dixon K.A., Tailor R.C. Interaction between vascularized lymph node transfer and recipient lymphatics after lymph node dissection-a pilot study in a canine model. *J Surg Res*, 2016, Vol. 204(2), pp. 418-427. doi: 10.1016/j.jss.2016.05.029.
13. Viitanen T.P., Visuri M.T., Hartiala P., Mäki M.T., Seppänen M.P., Suominen E.A., Saaristo A.M. Lymphatic vessel function and lymphatic growth factor secretion after microvascular lymph node transfer in lymphedema patients. *Plast Reconstr Surg Glob Open*, 2013, Vol. 1(2), pp. 1-9. doi: 10.1097/GOX.0b013e318293a532.
14. Executive Committee of the International Society of Lymphology. The diagnosis and treatment of peripheral lymphedema: 2020 Consensus Document of the International Society of Lymphology. *Lymphology*, 2020, Vol. 53(1), pp. 3-19.
15. Allen R.J. Jr, Cheng M.H. Lymphedema surgery: Patient selection and an overview of surgical techniques. *J Surg Oncol*, 2016, Vol. 113(8), pp. 923-931.
16. Gasteratos K., Morsi-Yeroyannis A., Vlachopoulos N.C., Spyropoulou G.A., Del Corral G., Chaiyasate K. Microsurgical techniques in the treatment of breast cancer-related lymphedema: a systematic review of efficacy and patient outcomes. *Breast Cancer*, 2021, Vol. 28(5), pp. 1002-1015. doi: 10.1007/s12282-021-01274-5.

Plast Surg. – 2018. – Vol. 32, №1. – P. 28-35. doi: 10.1055/s-0038-1632401.
12. Suami H., Scaglioni M.F., Dixon K.A., Tailor R.C. Interaction between vascularized lymph node transfer and recipient lymphatics after lymph node dissection-a pilot study in a canine model // J Surg Res. – 2016. – Vol. 204, №2. – P. 418-427. doi: 10.1016/j.jss.2016.05.029.
13. Viitanen T.P., Visuri M.T., Hartiala P., Mäki M.T., Seppänen M.P., Suominen E.A., Saaristo A.M. Lymphatic vessel function and lymphatic growth factor secretion after microvascular lymph node transfer in lymphedema patients // Plast Reconstr Surg Glob Open. – 2013. – Vol. 1, №2. – P. 1-9. doi: 10.1097/GOX.0b013e318293a532.
14. Executive Committee of the International Society of Lymphology. The diagnosis and treatment of peripheral lymphedema: 2020 Consensus Document of the International Society of Lymphology // Lymphology. – 2020. – Vol. 53, №1. – P. 3-19.
15. Allen R.J. Jr, Cheng M.H. Lymphedema surgery: Patient selection and an overview of surgical techniques // J Surg Oncol. – 2016. – Vol. 113, №8. – P. 923-931.
16. Gasteratos K., Morsi-Yeroyannis A., Vlachopoulos N.C., Spyropoulou G.A., Del Corral G., Chaiyasate K. Microsurgical techniques in the treatment of breast cancer-related lymphedema: a systematic review of efficacy and patient outcomes // Breast Cancer. – 2021. – Vol. 28, №5. – P. 1002-1015. doi: 10.1007/s12282-021-01274-5.